



Layered piezoelectric structures with arbitrary acoustic termination impedances

Stefan Braun,^{1,a)}  Helmut Nowotny,² Ewald Benes,³ and Martin Gröschl³ 

¹*Institute of Fluid Mechanics and Heat Transfer, Technische Universität Wien, 1060 Vienna, Austria*

²*Institute of Theoretical Physics, Technische Universität Wien, 1040 Vienna, Austria*

³*Institute of Applied Physics, Technische Universität Wien, 1040 Vienna, Austria*

ABSTRACT:

Multilayer piezoelectric transducers and resonators are widely used for generating propagating and standing acoustic waves as well as for sensor devices. More recently, layered piezoelectric structures based on thin film technology became increasingly important for electromechanical filters used in mobile phones. As a consequence, analytical mathematical modeling of such structures is of high interest. In this paper, a general rigorous transfer matrix description for one-dimensional (1D) layered structures consisting of piezoelectric, visco-elastic, and dielectric layers of arbitrary number is introduced to characterize the electrical and mechanical behavior of a general piezoelectric transducer or resonator with two electrodes and arbitrary acoustic termination impedances (Rig-1D-model). This model is the most general 1D analytical description of layered piezoelectric structures available and can be used for the characterization of various composite transducer and resonant sensor applications. Considered in detail are layered structures with the technically important cases of only one electromechanically coupled mode, and the structure at one or both outer surfaces is in contact with semi-infinite media. For such devices, it is shown how the frequency dependence of the total electrical admittance and spatial dependence of the displacements can be calculated.

© 2023 Author(s). All article content, except where otherwise noted, is licensed under a Creative Commons Attribution (CC BY) license (<http://creativecommons.org/licenses/by/4.0/>). <https://doi.org/10.1121/10.0017600>

(Received 28 September 2022; revised 25 January 2023; accepted 23 February 2023; published online 16 March 2023)

[Editor: Wonkyu Moon]

Pages: 1733–1753

I. INTRODUCTION

From a historical point of view, the first descriptions of layered piezoelectric structures were based on electrical transmission line analogies.^{1–4} The electrical network multimode representations for arrangements of piezoelectric plates consist of eight-port models, in particular, of six mechanical and two electrical ports. For the electromechanical characterization of stacked structures, the mechanical ports have to be interconnected via fictive transformers to model the coupling between the three eigenmodes. This description has the advantage of being somehow pictorial—at least for an electrical engineer—but requires involved electrical network analysis and the use of an electro-acoustical analogy.²

In the subsequent development, an important milestone was the introduction of a general 8×8 transfer matrix description of arbitrarily oriented layered piezoelectric resonator structures.⁵ In this so-called one-dimensional (1D) description, the physical quantities are not necessarily limited, only their location dependence is limited. In each plane $x_\nu = \text{constant}$, the physical quantities have the same value regardless of the considered location in this plane, that is, they depend only on the coordinate x_ν . The direction of x_ν corresponds to the thickness direction of the piezoelectric plate. This restricted spatial dependence of the physical variables lead to a simplification of the governing equations. For example, the stress vector

component, $c_{ijkl}\partial_i\partial_l u_k(x_1, x_2, x_3)$, simplifies to $c_{\nu jk\nu}\partial_\nu\partial_\nu u_k(x_\nu)$ for a chosen value ν . These simplifications allow the analytical solution of the equations of motion for a piezoelectric plate as shown in the work of Nowotny and Benes.⁵ The predictive results delivered by this so-called 1D model are in good to excellent agreement with measurement results from various practical piezoelectric transducer, resonator, and filter structures, especially in thin-film applications, i.e., when the thicknesses of the considered (exciting/active and anisotropic) layers are much smaller than their lateral dimensions or certain measures (“energy trapping”) prevent mode coupling (induced, e.g., by the device clamping at the edges).

In a further development step, the original restriction to two electrodes could be extended to the treatment of an arbitrary number of electrodes by also representing the electrode layers by a matrix description.⁶ The model was derived without using any electro-acoustical analogies as an exact analytical solution of the governing differential equations supplemented by their appropriate boundary conditions at the terminating surfaces and electrical port. In the approaches by Nowotny and Benes⁵ and Nowotny *et al.*⁶ for the outer terminating surfaces of the stack, the boundary condition for resonators with free end planes, i.e., vanishing mechanical stress, was used. In some applications, this condition was replaced by the complementary resonator boundary condition of fixed end planes (vanishing displacement).⁷ A general solution of the problem in closed form for any stacking sequence of layers was obtained, where each layer

^{a)}Electronic mail: stefan.braun@tuwien.ac.at

is characterized by the following parameters: layer thickness, mass density, effective elastic constants, piezoelectric constants, dielectric constants, and viscosity as a measure of the electromechanical losses. This 1D model allowed the calculation of the electrical admittance appearing between the electrodes for any frequency by performing only simple matrix multiplications and inherently covered the general case of multimode excitations and their coupling effects.

In summary, the work of Nowotny and Benes⁵ allowed the determination of the entire frequency spectrum of those composite resonators for the resonator boundary condition cases of free and fixed outer surfaces.

A. Previous applications

Because in most application cases only two electrodes are present, the previous work of Nowotny and Benes⁵ was widely used in numerous fields ranging from

- (a) resonant ultrasonic field generation in liquids for particle separation technologies, ultrasonic cell filters for perfusion-bioreactors, as well as for other ultrasonic standing wave (USW) devices^{8,9} over
- (b) resonant sensors, e.g., for quartz-crystal thin film thickness monitors,^{10,11}
- (c) electric filter applications, especially for mobile phones, where the piezoelectric resonator layer (e.g., TiN) is acoustic wave reflective face-mounted by the use of quarter-wavelength acoustic impedance transformation layers between the substrate and resonator.^{12–18} to
- (d) acoustic transmission and delay lines.^{9,19–21}

B. Recent applications

In the present paper, the rigorous model of Nowotny and Benes⁵ is extended to cover the most general boundary condition of terminating the outer planes of the sandwich structure by semi-infinite media of arbitrary acoustic impedance. The description introduced below with code name Rig-1D-model is herewith the most general 1D analytical description of layered piezoelectric structures available and can be used for the modeling of any composite transducer and resonant sensor application. Consequently, the scope of possible applications of the Rig-1D-model is further extended to

- (a) transducers with matching and backing layers, e.g., for SONAR and ultrasonic imaging^{22–26} and
- (b) resonant sensors in contact with fluids, e.g., viscosity, density, or speed of sound sensors.^{7,26–36}

II. GENERAL 1D MATHEMATICAL MODEL

For the Rig-1D-model presented here, we adopt the transfer matrix formalism introduced in Nowotny *et al.*⁶ and apply it to the case of two electrodes. Although this finally leads to the description of two electrodes as given in Nowotny and Benes,⁵ the more recent paper⁶ is chosen as a starting point because the structure of the equations used in Ref. 6 is more suitable for our present approach.

The thickness direction of the layered piezoelectric structure is denoted as x_ν in accordance with the IEEE Standard on Piezoelectricity.³⁷ In particular, for a Y-cut quartz $\nu = 2$, which means that the thickness direction is the y-direction, whereas for a piezo-ceramic material $\nu = 3$, the thickness direction is the z-direction. If the piezoelectric material exhibits only one displacement eigen-direction, as in the two cases just mentioned, the transfer matrix calculations simplify because the matrix dimensions reduce from 8×8 to 4×4 due to the fact that the displacement is aligned with or is perpendicular to the axis direction, x_ν . This reduction was used in many applications of the transfer matrix model; see, e.g., Refs. 38–41. Consequently, these cases of technical importance will be considered in more detail below.

A. Transfer matrix of one film layer

Regarding a plate located between $x_\nu = 0$ and $x_\nu = l$ (see Fig. 1), we can calculate the boundary values of the displacement vector (Cartesian) components, u_i , the stress vector components, T_j , with $i, j = 1, 2, 3$, the electric potential, φ , and the electric displacement, D_ν , at $x_\nu = l$ as linear functions of the boundary values at $x_\nu = 0$ (for details, see the work of Nowotny and Benes⁵). Considering solutions with time dependence, $e^{+j\omega t}$ (time harmonic solutions), these linear relations between the boundary values at the two sides of the plate can be written in the form (see Ref. 6)

$$\begin{pmatrix} u_1 \\ u_2 \\ u_3 \\ T_1 \\ T_2 \\ T_3 \\ \varphi \\ D_\nu \end{pmatrix}_{x_\nu=l} = \underbrace{\begin{pmatrix} M^{uu}_{11} & M^{uu}_{12} & M^{uu}_{13} & M^{uT}_{11} & M^{uT}_{12} & M^{uT}_{13} & 0 & M^{uD}_1 \\ M^{uu}_{21} & M^{uu}_{22} & M^{uu}_{23} & M^{uT}_{21} & M^{uT}_{22} & M^{uT}_{23} & 0 & M^{uD}_2 \\ M^{uu}_{31} & M^{uu}_{32} & M^{uu}_{33} & M^{uT}_{31} & M^{uT}_{32} & M^{uT}_{33} & 0 & M^{uD}_3 \\ M^{Tu}_{11} & M^{Tu}_{12} & M^{Tu}_{13} & M^{TT}_{11} & M^{TT}_{12} & M^{TT}_{13} & 0 & M^{TD}_1 \\ M^{Tu}_{21} & M^{Tu}_{22} & M^{Tu}_{23} & M^{TT}_{21} & M^{TT}_{22} & M^{TT}_{23} & 0 & M^{TD}_2 \\ M^{Tu}_{31} & M^{Tu}_{32} & M^{Tu}_{33} & M^{TT}_{31} & M^{TT}_{32} & M^{TT}_{33} & 0 & M^{TD}_3 \\ M^{\varphi u}_1 & M^{\varphi u}_2 & M^{\varphi u}_3 & M^{\varphi T}_1 & M^{\varphi T}_2 & M^{\varphi T}_3 & 1 & M^{\varphi D} \\ 0 & 0 & 0 & 0 & 0 & 0 & 0 & 1 \end{pmatrix}}_{\mathbf{M}} \begin{pmatrix} u_1 \\ u_2 \\ u_3 \\ T_1 \\ T_2 \\ T_3 \\ \varphi \\ D_\nu \end{pmatrix}_{x_\nu=0}, \quad (1)$$

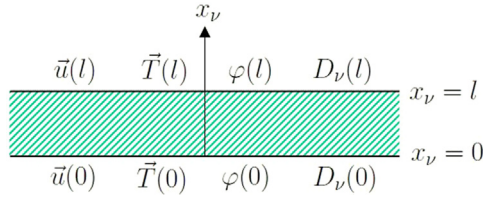


FIG. 1. (Color online) Boundary values for a single layer of thickness, l .

with an 8×8 transfer matrix, \mathbf{M} . The different parts of the complete 8×8 transfer matrix are given by the following formulas with the Cartesian components $i, j, k, l = 1, 2, 3$ (see Ref. 6):

$$M_{ij}^{uu} = \sum_n \beta_i^{(n)} \beta_j^{(n)} \cos \alpha^{(n)} l \omega, \tag{2}$$

$$M_{il}^{uT} = \sum_n \beta_i^{(n)} \beta_l^{(n)} \frac{1}{z^{(n)} \omega} \sin \alpha^{(n)} l \omega, \tag{3}$$

$$M_{kj}^{Tu} = - \sum_n \beta_k^{(n)} \beta_j^{(n)} z^{(n)} \omega \sin \alpha^{(n)} l \omega, \tag{4}$$

$$M_{kl}^{TT} = M_{kl}^{uu}, \tag{5}$$

$$M_i^{uD} = \sum_n \beta_i^{(n)} \frac{k^{(n)}}{\sqrt{\epsilon_{\nu\nu} \rho} \omega} \sin \alpha^{(n)} l \omega, \tag{6}$$

$$M_k^{TD} = - \sum_n \beta_k^{(n)} \frac{k^{(n)} z^{(n)}}{\sqrt{\epsilon_{\nu\nu} \rho}} (1 - \cos \alpha^{(n)} l \omega), \tag{7}$$

$$M_j^{\phi u} = M_j^{TD}, \tag{8}$$

$$M_l^{\phi T} = M_l^{uD}, \tag{9}$$

$$M^{\phi D} = - \frac{l}{\epsilon_{\nu\nu}} \left(1 - \sum_n \frac{k^{(n)2}}{\alpha^{(n)} l \omega} \sin \alpha^{(n)} l \omega \right). \tag{10}$$

In these equations, l and ω denote the thickness of the layer and circular frequency, respectively. All of the other variables can be calculated from the material constants mass density, ρ , elastic stiffness constant, $c_{\nu j k \nu}$ (for constant electric field, E ; full notation, $c_{\nu j k \nu}^E$), piezoelectric constant, $e_{\nu \nu j}$, and dielectric constant, $\epsilon_{\nu \nu}$ (for constant strain, S ; full notation, $\epsilon_{\nu \nu}^S$). From the piezoelectrically stiffened elastic constant tensor (see Refs. 37 and 42),

$$\bar{c}_{\nu j k \nu} = c_{\nu j k \nu} + \frac{e_{\nu \nu j} e_{\nu \nu k}}{\epsilon_{\nu \nu}}, \tag{11}$$

one can calculate the three eigenvalues, $\bar{c}^{(n)}$, and the corresponding three eigenvectors, $\beta_j^{(n)}$, such that

$$\bar{c}_{\nu j k \nu} \beta_k^{(n)} = \bar{c}^{(n)} \beta_j^{(n)}, \quad n = 1, 2, 3. \tag{12}$$

In the calculations, we make use of the Einstein summation convention over double Latin indices; the Greek index, ν , remains fixed. The slowness, $\alpha^{(n)}$, is given by

$$\alpha^{(n)} = \sqrt{\frac{\rho}{\bar{c}^{(n)}}}, \tag{13}$$

the acoustic impedance per cross-sectional area, $z^{(n)}$, is given by

$$z^{(n)} = \sqrt{\bar{c}^{(n)} \rho}, \tag{14}$$

and the dimensionless piezoelectric coupling factor, $k^{(n)}$, is given by

$$k^{(n)} = \frac{e_{\nu \nu j} \beta_j^{(n)}}{\sqrt{\bar{c}^{(n)} \epsilon_{\nu \nu}}}. \tag{15}$$

If we consider materials with elastic and dielectric losses, we can use complex material constants as shown by Holland.⁴³ For a time dependence of the form $e^{+j\omega t}$, as usually used by electrical engineers, this means that the imaginary part has to be taken as positive for the elastic stiffness constant, c , and negative for the dielectric constant, ϵ .

For the further calculations, we write Eq. (1) in a more compact vector notation as

$$\begin{pmatrix} \vec{u} \\ \vec{T} \\ \phi \\ D_\nu \end{pmatrix}_{x_\nu=l} = \begin{pmatrix} \mathbf{M}^{uu} & \mathbf{M}^{uT} & 0 & \vec{M}^{uD} \\ \mathbf{M}^{Tu} & \mathbf{M}^{TT} & 0 & \vec{M}^{TD} \\ \vec{M}^{\phi u} & \vec{M}^{\phi T} & 1 & M^{\phi D} \\ 0 & 0 & 0 & 1 \end{pmatrix} \begin{pmatrix} \vec{u} \\ \vec{T} \\ \phi \\ D_\nu \end{pmatrix}_{x_\nu=0}. \tag{16}$$

B. Transfer matrix of a layered stack

The physical boundary condition for slip-free interfacing surfaces of two films is the equality of the values of the variables, \vec{u} , \vec{T} , ϕ , D_ν , at the interface, which we have chosen as termination parameters for the transfer matrix description. Therefore, in the transfer matrix description, the connection between two films appears to be a matrix multiplication of the single transfer matrices. If the general form of the transfer matrix as given by Eq. (1) is used for each single film of a stack, it can be shown that this general form is conserved after matrix multiplication.⁵ Consequently, the total transfer matrix for an arbitrary number of films without an electrode in between is of the same form as the general transfer matrix of a single film.

According to Eq. (1), the boundary values, D_ν , are equal for both sides of a dielectric film. However, this is not the case for an electrically conducting electrode. On both sides of such an electrode, the values of D_ν , in general, are different and will be denoted as D_ν^+ and D_ν^- (see Fig. 2). The difference, $D_\nu^+ - D_\nu^-$, is related to the electric charge per

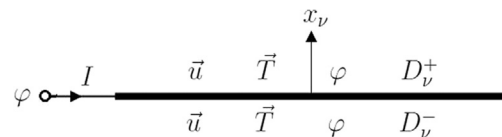


FIG. 2. Boundary values for an electrode.

unit area on the electrode and from Maxwell's equations, we obtain the electric current, I , flowing to the electrode as

$$I = j\omega A(D_\nu^+ - D_\nu^-), \quad (17)$$

where A denotes the area of the electrode. Equation (17) shows that the boundary values of D_ν directly depend on the electric current, I , flowing to this electrode. We can use Eq. (17) to connect the values $(\vec{u}, \vec{T}, \varphi, D_\nu)$ on both sides, E^+ and E^- , of the electrode

$$\begin{pmatrix} \vec{u} \\ \vec{T} \\ \varphi \\ D_\nu \end{pmatrix}_{E^+} = \begin{pmatrix} \vec{u} \\ \vec{T} \\ \varphi \\ D_\nu \end{pmatrix}_{E^-} + \begin{pmatrix} 0 \\ 0 \\ 0 \\ 1 \end{pmatrix} \frac{I}{j\omega A}. \quad (18)$$

C. Composite structure with two electrodes

If an ordered stack with two electrodes (see Fig. 3) is considered, for both electrodes, the equation

$$\begin{pmatrix} \vec{u} \\ \vec{T} \\ \varphi \\ D_\nu \end{pmatrix}_{x_\nu=b} = \mathbf{M}_{GQF} \begin{pmatrix} \vec{u} \\ \vec{T} \\ \varphi \\ D_\nu \end{pmatrix}_{x_\nu=a} + \mathbf{M}_{GQ} \begin{pmatrix} 0 \\ 0 \\ 0 \\ 1 \end{pmatrix} \frac{I_0}{j\omega A} + \mathbf{M}_G \begin{pmatrix} 0 \\ 0 \\ 0 \\ 1 \end{pmatrix} \frac{I_1}{j\omega A} \quad (19)$$

is obtained by using Eq. (18). Here, the notation,

$$\mathbf{M}_{GQF} = \mathbf{M}_G \mathbf{M}_Q \mathbf{M}_F, \quad \mathbf{M}_{GQ} = \mathbf{M}_G \mathbf{M}_Q, \quad (20)$$

is used whereby the transfer matrix for a stack without an electrode is given by the matrix product of the single layer transfer matrices of all of the layers within the stack (the matrix multiplication always occurs according to the order in the stack).

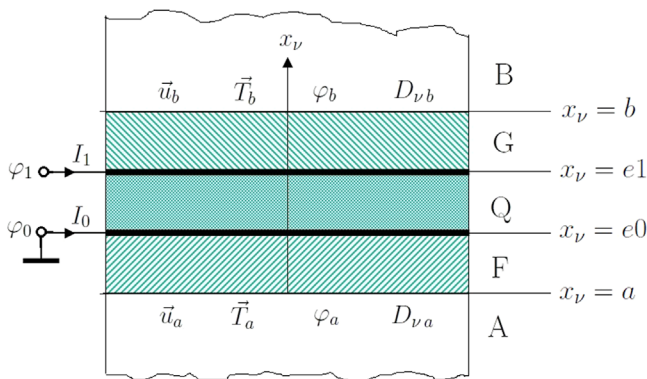


FIG. 3. (Color online) The composite structure with layered stack, Q , between two electrodes and layered stack, F , with boundary medium, A , on one side and layered stack, G , with boundary medium, B , at the other side.

Writing Eq. (19) more explicitly [cf. Eq. (16)], we obtain

$$\begin{aligned} \vec{u}_b &= \mathbf{M}_{GQF}^{uu} \vec{u}_a + \mathbf{M}_{GQF}^{uT} \vec{T}_a + \vec{M}_{GQF}^{uD} D_{\nu a} \\ &+ \vec{M}_{GQ}^{uD} \frac{I_0}{j\omega A} + \vec{M}_G^{uD} \frac{I_1}{j\omega A}, \end{aligned} \quad (21)$$

$$\begin{aligned} \vec{T}_b &= \mathbf{M}_{GQF}^{Tu} \vec{u}_a + \mathbf{M}_{GQF}^{TT} \vec{T}_a + \vec{M}_{GQF}^{TD} D_{\nu a} \\ &+ \vec{M}_{GQ}^{TD} \frac{I_0}{j\omega A} + \vec{M}_G^{TD} \frac{I_1}{j\omega A}, \end{aligned} \quad (22)$$

$$\begin{aligned} \varphi_b &= \vec{M}_{GQF}^{\varphi u} \vec{u}_a + \vec{M}_{GQF}^{\varphi T} \vec{T}_a + \varphi_a + M_{GQF}^{\varphi D} D_{\nu a} \\ &+ M_{GQ}^{\varphi D} \frac{I_0}{j\omega A} + M_G^{\varphi D} \frac{I_1}{j\omega A}, \end{aligned} \quad (23)$$

$$D_{\nu b} = D_{\nu a} + \frac{I_0}{j\omega A} + \frac{I_1}{j\omega A}. \quad (24)$$

For the boundary media A and B , the relations $D_{\nu b} = D_{\nu a} = 0$ hold and, furthermore, the equation $I_0 = -I_1$ applies.

D. Boundary medium conditions

As the non-piezoelectric boundary media A and B are assumed to be extended semi-infinitely, only outgoing waves can be present. Outgoing waves in medium A as solution of the equation of motion [see Eq. (5.21) on p. 36 of Tiersten⁴²],

$$c_{vij\nu} \partial_\nu \partial_\nu u_j = \rho \ddot{u}_i, \quad i = 1, 2, 3, \quad (25)$$

are given by

$$u_{iA}(x_\nu, t) = \sum_n C_A^{(n)} \beta_{iA}^{(n)} e^{j\omega \alpha_A^{(n)} x_\nu} e^{j\omega t}, \quad (26)$$

where $C_A^{(n)}$ are the displacement amplitudes for the three different eigenmodes described by the eigenvectors $\beta_{iA}^{(n)}$ of Eq. (12),

$$c_{vij\nu A} \beta_{jA}^{(n)} = c_A^{(n)} \beta_{iA}^{(n)}, \quad n = 1, 2, 3,$$

and the slowness, $\alpha_A^{(n)}$, according to Eq. (13),

$$\alpha_A^{(n)} = \sqrt{\frac{\rho}{c_A^{(n)}}}.$$

The calculation of the stress,

$$T_{vi} = c_{vij\nu} \partial_\nu u_j,$$

gives, in a first step,

$$\begin{aligned} T_{iA} &= c_{vij\nu A} \sum_n C_A^{(n)} \beta_{jA}^{(n)} j\omega \alpha_A^{(n)} e^{j\omega \alpha_A^{(n)} x_\nu} e^{j\omega t} \\ &= j\omega \sum_n C_A^{(n)} c_A^{(n)} \beta_{iA}^{(n)} \alpha_A^{(n)} e^{j\omega \alpha_A^{(n)} x_\nu} e^{j\omega t} \\ &= j\omega \sum_n c_A^{(n)} \alpha_A^{(n)} \beta_{iA}^{(n)} \sum_m \delta_{nm} C_A^{(m)} e^{j\omega \alpha_A^{(m)} x_\nu} e^{j\omega t}. \end{aligned}$$

Using the orthogonality relation of the eigenvectors, $\beta_{iA}^{(n)}$,

$$\beta_{jA}^{(n)} \beta_{jA}^{(m)} = \delta_{nm},$$

and the definition of the acoustic impedance per cross-sectional area, $z_A^{(n)}$ [see Eqs. (13) and (14)], is

$$z_A^{(n)} = \sqrt{c_A^{(n)} \rho_A} = c_A^{(n)} \sqrt{\frac{\rho_A}{c_A^{(n)}}} = c_A^{(n)} \alpha_A^{(n)},$$

one obtains

$$T_{iA} = j\omega \sum_n z_A^{(n)} \beta_{iA}^{(n)} \beta_{jA}^{(n)} \sum_m C_A^{(m)} \beta_{jA}^{(m)} e^{j\omega \alpha_A^{(m)} x_\nu} e^{j\omega t}. \quad (27)$$

The sum over m now exactly represents the displacement, u_{jA} [see Eq. (26)]. Therefore, one can write

$$T_{iA}(x_\nu, t) = j\omega \sum_n z_A^{(n)} \beta_{iA}^{(n)} \beta_{jA}^{(n)} u_{jA}(x_\nu, t). \quad (28)$$

For the further calculations, it is essential to note that the stress vector, \vec{T} , is directly connected to the displacement vector, \vec{u} . As a consequence, a relation between the mechanical variable, \vec{u} , and the electric variable, φ , can be obtained.

Equation (28) can be written in short notation as

$$\vec{T}_A(x_\nu, t) = j\omega \mathbf{N}_A^{Tu} \vec{u}_A(x_\nu, t), \quad (29)$$

with the 3×3 matrix,

$$(\mathbf{N}_A^{Tu})_{ij} = \sum_n z_A^{(n)} \beta_{iA}^{(n)} \beta_{jA}^{(n)}. \quad (30)$$

In analogy, for outgoing waves in medium B , the ansatz,

$$u_{iB}(x_\nu, t) = \sum_n C_B^{(n)} \beta_{iB}^{(n)} e^{-j\omega \alpha_B^{(n)} x_\nu} e^{j\omega t}, \quad (31)$$

is used for the displacement. Hence, the stress can be specified to

$$\vec{T}_B(x_\nu, t) = -j\omega \mathbf{N}_B^{Tu} \vec{u}_B(x_\nu, t), \quad (32)$$

with the 3×3 matrix,

$$(\mathbf{N}_B^{Tu})_{ij} = \sum_n z_B^{(n)} \beta_{iB}^{(n)} \beta_{jB}^{(n)}. \quad (33)$$

We now use Eqs. (21)–(24) to obtain a relationship between the values of the electric currents and the mechanical displacements at the surfaces $x_\nu = a$ and $x_\nu = b$.

Using $D_{\nu b} = D_{\nu a} = 0$ and $I_0 = -I_1$ in Eqs. (21) and (22), the following connection between the boundary values of the displacement at the surfaces next to the outside media B and A can be obtained:

$$\vec{u}_b = \left(\mathbf{M}_{GQF}^{uu} + \mathbf{M}_{GQF}^{uT} j\omega \mathbf{N}_A^{Tu} \right) \vec{u}_a - \left(\vec{M}_{GQ}^{uD} - \vec{M}_G^{uD} \right) \frac{I_1}{j\omega A}, \quad (34)$$

$$-j\omega \mathbf{N}_B^{Tu} \vec{u}_b = \left(\mathbf{M}_{GQF}^{Tu} + \mathbf{M}_{GQF}^{TT} j\omega \mathbf{N}_A^{Tu} \right) \vec{u}_a - \left(\vec{M}_{GQ}^{TD} - \vec{M}_G^{TD} \right) \frac{I_1}{j\omega A}. \quad (35)$$

An elimination of the displacement, \vec{u}_b , from Eqs. (34) and (35) is easily possible and yields

$$-j\omega \mathbf{N}_B^{Tu} \left[\left(\mathbf{M}_{GQF}^{uu} + \mathbf{M}_{GQF}^{uT} j\omega \mathbf{N}_A^{Tu} \right) \vec{u}_a - \left(\vec{M}_{GQ}^{uD} - \vec{M}_G^{uD} \right) \frac{I_1}{j\omega A} \right] = \left(\mathbf{M}_{GQF}^{Tu} + \mathbf{M}_{GQF}^{TT} j\omega \mathbf{N}_A^{Tu} \right) \vec{u}_a - \left(\vec{M}_{GQ}^{TD} - \vec{M}_G^{TD} \right) \frac{I_1}{j\omega A}. \quad (36)$$

Equation (36) represents a direct relation between the displacement, \vec{u}_a , at the interface, $x_\nu = a$, and the electric current, I_1 , flowing to the resonator,

$$\vec{u}_a = \left[\mathbf{M}_{GQF}^{Tu} + j\omega \mathbf{M}_{GQF}^{TT} \mathbf{N}_A^{Tu} + j\omega \mathbf{N}_B^{Tu} \mathbf{M}_{GQF}^{uu} - \omega^2 \mathbf{N}_B^{Tu} \mathbf{M}_{GQF}^{uT} \mathbf{N}_A^{Tu} \right]^{-1} \times \left[\vec{M}_{GQ}^{TD} - \vec{M}_G^{TD} + j\omega \mathbf{N}_B^{Tu} \left(\vec{M}_{GQ}^{uD} - \vec{M}_G^{uD} \right) \right] \frac{I_1}{j\omega A}. \quad (37)$$

Here, the exponent of the first factor on the right-hand side, $[\cdot \cdot]^{-1}$, denotes matrix inversion (not to be confused with the reciprocal). This direct relationship between electric and mechanical variables is a consequence of the presence of piezoelectric materials in the stack between the electrodes. Only film layers with nonvanishing electromechanical coupling factors, k , have nonzero transfer matrix elements, \vec{M}_{GQ}^{TD} , \vec{M}_G^{TD} , \vec{M}_{GQ}^{uD} , and \vec{M}_G^{uD} , occurring in the last bracket of Eq. (37).

E. Electric admittance of a composite structure

To obtain a relationship between the electric currents and electric potentials at the electrodes, potential equations are needed. The transfer matrix connections between the boundary surface at $x_\nu = a$ and electrodes at $x_\nu = e1$ and $x_\nu = e0$ are given by [see the analogous connection given by Eq. (19)]

$$\begin{pmatrix} \vec{u} \\ \vec{T} \\ \varphi \\ D_\nu \end{pmatrix}_{x_\nu=e1} = \mathbf{M}_{QF} \begin{pmatrix} \vec{u} \\ \vec{T} \\ \varphi \\ D_\nu \end{pmatrix}_{x_\nu=a} + \mathbf{M}_Q \begin{pmatrix} 0 \\ 0 \\ 0 \\ 1 \end{pmatrix} \frac{I_0}{j\omega A}, \quad (38)$$

$$\begin{pmatrix} \vec{u} \\ \vec{T} \\ \varphi \\ D_\nu \end{pmatrix}_{x_\nu=e0} = \mathbf{M}_F \begin{pmatrix} \vec{u} \\ \vec{T} \\ \varphi \\ D_\nu \end{pmatrix}_{x_\nu=a}. \quad (39)$$

From Eqs. (38) and (39), we obtain explicit formulas for the electric potentials, φ_1 and φ_0 , such that

$$\varphi_1 = \left(\vec{M}_{QF}^{\varphi u} + j\omega \vec{M}_{QF}^{\varphi T} \mathbf{N}_A^{Tu} \right) \vec{u}_a + \varphi_a + M_Q^{\varphi D} \frac{I_0}{j\omega A}, \quad (40)$$

$$\varphi_0 = \left(\vec{M}_F^{\varphi u} + j\omega \vec{M}_F^{\varphi T} \mathbf{N}_A^{Tu} \right) \vec{u}_a + \varphi_a. \quad (41)$$

If we assume that electrode 0 is grounded ($\varphi_0 = 0$), the boundary potential value, φ_a , can be calculated from Eq. (41) as a function of \vec{u}_a ,

$$\varphi_a = - \left(\vec{M}_F^{\varphi u} + j\omega \vec{M}_F^{\varphi T} \mathbf{N}_A^{Tu} \right) \vec{u}_a. \quad (42)$$

Using Eq. (42) for the calculation of φ_1 results in

$$\varphi_1 = M_Q^{\varphi D} \frac{I_0}{j\omega A} + \left(\vec{M}_{QF}^{\varphi u} + j\omega \vec{M}_{QF}^{\varphi T} \mathbf{N}_A^{Tu} - \vec{M}_F^{\varphi u} - j\omega \vec{M}_F^{\varphi T} \mathbf{N}_A^{Tu} \right) \vec{u}_a. \quad (43)$$

This is a linear relation between the electric potential, φ_1 , and the electric current, I_1 [see Eq. (37) for \vec{u}_a and use $I_0 = -I_1$], which defines the electric impedance, $Z(\omega)$, of the piezoelectric resonator as

$$\varphi_1 = Z(\omega) I_1. \quad (44)$$

Therefore, from Eq. (43) and using Eq. (37), the following formula for the electric impedance is obtained:

$$Z(\omega) = \frac{1}{j\omega A} \left[-M_Q^{\varphi D} + \left(\vec{M}_{QF}^{\varphi u} + j\omega \vec{M}_{QF}^{\varphi T} \mathbf{N}_A^{Tu} - \vec{M}_F^{\varphi u} - j\omega \vec{M}_F^{\varphi T} \mathbf{N}_A^{Tu} \right) \times \left(\mathbf{M}_{GQF}^{Tu} + j\omega \mathbf{M}_{GQF}^{TT} \mathbf{N}_A^{Tu} + j\omega \mathbf{N}_B^{Tu} \mathbf{M}_{GQF}^{uu} - \omega^2 \mathbf{N}_B^{Tu} \mathbf{M}_{GQF}^{uT} \mathbf{N}_A^{Tu} \right)^{-1} \times \left(\vec{M}_{GQ}^{TD} - \vec{M}_G^{TD} + j\omega \mathbf{N}_B^{Tu} \left(\vec{M}_{GQ}^{uD} - \vec{M}_G^{uD} \right) \right) \right]. \quad (45)$$

F. Spatial course of the displacement

To get the spatial x_ν -dependence of the quantities displacement, $\vec{u}(x_\nu)$, stress, $\vec{T}(x_\nu)$, electric potential, $\varphi(x_\nu)$, and electric displacement, $D_\nu(x_\nu)$, we only need to know the starting values of these variables at the surface, $x_\nu = a$, and then we can use the transfer matrices for an arbitrarily chosen location, x_ν . Depending on the chosen value of x_ν , one or more stacked layers need to be taken into account to calculate the values $\vec{u}(x_\nu)$, $\vec{T}(x_\nu)$, $\varphi(x_\nu)$, and $D_\nu(x_\nu)$. The boundary values, \vec{u}_a , \vec{T}_a , φ_a , and $D_{\nu a}$, depend on the driving

voltage, φ_1 , only. The displacement, \vec{u}_a , is given by Eq. (37) using $I_1 = \varphi_1/Z(\omega)$, the stress, \vec{T}_a , is computed from Eq. (29) using \vec{u}_a , the potential, φ_a , is given by Eq. (42), and the electric displacement, $D_{\nu a}$, is zero.

Using these boundary values, all of the x_ν -dependent quantities can be calculated such that

$$\begin{pmatrix} \vec{u} \\ \vec{T} \\ \varphi \\ D_\nu \end{pmatrix}_{x_\nu} = \mathbf{M}_{x_\nu a} \begin{pmatrix} \vec{u}_a \\ \vec{T}_a \\ \varphi_a \\ 0 \end{pmatrix} - (\mathbf{M}_{x_\nu e0} - \mathbf{M}_{x_\nu e1}) \begin{pmatrix} 0 \\ 0 \\ 0 \\ 1 \end{pmatrix} \frac{1}{j\omega A} \frac{\varphi_1}{Z(\omega)}. \quad (46)$$

Depending on the position, x_ν , the regarding contribution of the electrodes has to be included (for stack F no electrode, for stack Q the electrode zero, this means the transfer matrix, $\mathbf{M}_{x_\nu e0}$, and for stack G both electrodes, this means transfer matrices $\mathbf{M}_{x_\nu e0}$ and $\mathbf{M}_{x_\nu e1}$).

III. ONLY ONE ELECTROMECHANICALLY COUPLED MODE

A. 4 × 4 transfer matrix

If the crystallographic orientation of the active piezoelectric layer, reflected in the specific structure of the 8 × 8 transfer matrix, implies that an electric voltage applied to the electrodes can only excite mechanical displacement corresponding to one of the three eigenmodes, a reduction from the 8 × 8 transfer matrix to a 4 × 4 transfer matrix is possible. From all of the vectors, \vec{u} , \vec{T} , \vec{M}^{uD} , \vec{M}^{TD} , $\vec{M}^{\varphi u}$, $\vec{M}^{\varphi T}$, and all of the 3 × 3 matrices, \mathbf{M}^{uu} , \mathbf{M}^{uT} , \mathbf{M}^{Tu} , \mathbf{M}^{TT} , only one element is necessary for the calculation:

$$\begin{pmatrix} u \\ T \\ \varphi \\ D_\nu \end{pmatrix}_{x_\nu=l} = \begin{pmatrix} M^{uu} & M^{uT} & 0 & M^{uD} \\ M^{Tu} & M^{TT} & 0 & M^{TD} \\ M^{\varphi u} & M^{\varphi T} & 1 & M^{\varphi D} \\ 0 & 0 & 0 & 1 \end{pmatrix} \begin{pmatrix} u \\ T \\ \varphi \\ D_\nu \end{pmatrix}_{x_\nu=0}. \quad (47)$$

B. Electric admittance

The formula (45) for the electric impedance, $Z(\omega)$, simplifies to

$$Z(\omega) = \frac{1}{j\omega A} \left[-M_Q^{\varphi D} + \frac{\left(M_{QF}^{\varphi u} + j\omega z_A M_{QF}^{\varphi T} - M_F^{\varphi u} - j\omega z_A M_F^{\varphi T} \right) \left(M_{GQ}^{TD} - M_G^{TD} + j\omega z_B M_{GQ}^{uD} - j\omega z_B M_G^{uD} \right)}{M_{GQF}^{Tu} + j\omega \left(z_A M_{GQF}^{TT} + z_B M_{GQF}^{uu} \right) - \omega^2 z_A z_B M_{GQF}^{uT}} \right]. \quad (48)$$

Here, z_A and z_B denote the specific acoustic impedances of the boundary media, A and B , respectively.

Experimental results are usually specified in terms of the admittance, $Y(\omega) = 1/Z(\omega)$. A plot of $Y(\omega)$ is also used to determine the different harmonic resonance frequencies, f_{m-} , f_m , and f_{m+} of a piezoelectric resonator (see Fig. 5).

C. Mechanical displacement

For the calculation of the mechanical displacement, as a starting point, we need the boundary value, u_a , given in the general formula, Eq. (37). If the calculation can be performed with a 4×4 transfer matrix, this formula simplifies to

$$u_a = \frac{1}{j\omega A} \frac{\varphi_1}{Z(\omega)} \times \frac{M_{GQ}^{TD} - M_G^{TD} + j\omega z_B (M_{GQ}^{uD} - M_G^{uD})}{M_{GQF}^{Tu} + j\omega z_A M_{GQF}^{TT} + j\omega z_B M_{GQF}^{uu} - \omega^2 z_A z_B M_{GQF}^{uT}}. \tag{49}$$

IV. ONLY ONE PIEZOELECTRIC LAYER

If only one of the three eigenmodes in a single piezoelectric layer is excited, a 4×4 transfer matrix description is possible, and the elements of the transfer matrix are given by the following simplified relations:

$$M^{uu} = \cos \alpha\omega, \tag{50}$$

$$M^{uT} = \frac{1}{z\omega} \sin \alpha\omega, \tag{51}$$

$$M^{Tu} = -z\omega \sin \alpha\omega, \tag{52}$$

$$M^{TT} = M^{uu}, \tag{53}$$

$$M^{uD} = \sqrt{\frac{1}{\varepsilon\rho}} \frac{k}{\omega} \sin \alpha\omega, \tag{54}$$

$$M^{TD} = -\sqrt{\frac{1}{\varepsilon\rho}} k z (1 - \cos \alpha\omega), \tag{55}$$

$$M^{\varphi u} = M^{TD}, \tag{56}$$

$$M^{\varphi T} = M^{uD}, \tag{57}$$

$$M^{\varphi D} = -\frac{l}{\varepsilon} \left(1 - k^2 \frac{1}{\alpha l \omega} \sin \alpha l \omega \right). \tag{58}$$

In Eqs. (50)–(58), ε is the component, $\varepsilon_{\nu\nu}$, of the dielectric constant. With one component, c , of the elastic stiffness constant, $c_{\nu j k \nu}$, and one component, e , of the piezoelectric constant, $e_{\nu\nu j}$, the piezoelectrically stiffened elastic constant, \bar{c} , is given by

$$\bar{c} = c + \frac{e^2}{\varepsilon}. \tag{59}$$

This piezoelectrically stiffened elastic constant together with the mass density, ρ , is used for the calculation of the slowness,

$$\alpha = \sqrt{\frac{\rho}{\bar{c}}}. \tag{60}$$

The specific acoustic impedance, z , simplifies to

$$z = \sqrt{\bar{c}\rho}, \tag{61}$$

and the dimensionless piezoelectric coupling factor, k , is given by

$$k = \frac{e}{\sqrt{\bar{c}\varepsilon}}. \tag{62}$$

For a piezoelectric resonator with only one piezoelectric layer, Q , between the electrodes and boundary medium, A , at one side and boundary medium, B , at the other side (see Fig. 4), Eq. (48) for the electric impedance, $Z(\omega)$, can be simplified analytically such that

$$Z(\omega) = \frac{1}{j\omega A} \left[-M^{\varphi D} + \frac{(M^{\varphi u} + j\omega z_A M^{\varphi T})(M^{TD} + j\omega z_B M^{uD})}{M^{Tu} + j\omega(z_A M^{TT} + z_B M^{uu}) - \omega^2 z_A z_B M^{uT}} \right]. \tag{63}$$

Using Eqs. (50)–(58) results in

$$Z(\omega) = \frac{1}{j\omega A} \left[\frac{l}{\varepsilon} \left(1 - k^2 \frac{1}{\alpha l \omega} \sin \alpha l \omega \right) + \frac{1}{\varepsilon\rho} \frac{\left(-kz(1 - \cos \alpha\omega) + j\omega z_A \frac{k}{\omega} \sin \alpha\omega \right) \left(-kz(1 - \cos \alpha\omega) + j\omega z_B \frac{k}{\omega} \sin \alpha\omega \right)}{-z\omega \sin \alpha\omega + j\omega(z_A + z_B) \cos \alpha\omega - \omega z_A z_B \frac{\sin \alpha\omega}{z}} \right]. \tag{64}$$

This relation can be written as

$$Z(\omega) = \frac{1}{j\omega A} \frac{l}{\varepsilon} \left[1 - \frac{k^2}{\alpha\omega} \sin \alpha\omega - \frac{k^2}{\alpha\omega} \frac{(1 - \cos \alpha\omega - jz_a \sin \alpha\omega)(1 - \cos \alpha\omega - jz_b \sin \alpha\omega)}{\sin \alpha\omega - j(z_a + z_b) \cos \alpha\omega + z_a z_b \sin \alpha\omega} \right], \tag{65}$$

where

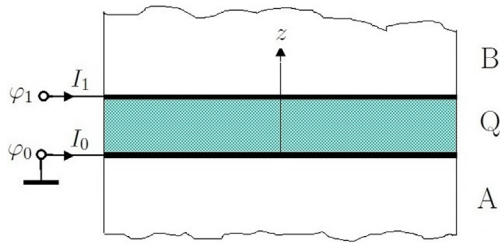


FIG. 4. (Color online) The resonator with one piezoelectric layer, Q , between two electrodes and boundary medium, A , at one side and boundary medium, B , at the other side.

$$z_a = \frac{z_A}{z} \quad \text{and} \quad z_b = \frac{z_B}{z}. \quad (66)$$

Combining the last two terms in the square brackets and using the capacitance, C_o , such that

$$C_o = \frac{A \varepsilon}{l}, \quad (67)$$

and the mean boundary acoustic impedance, z_{ab} , such that

$$z_{ab} = \frac{z_a + z_b}{2}, \quad (68)$$

we obtain

$$Z(\omega) = \frac{1}{j\omega C_o} \left[1 - \frac{2k^2}{\alpha l \omega} \frac{1 - \cos \alpha l \omega - j z_{ab} \sin \alpha l \omega}{(1 + z_a z_b) \sin \alpha l \omega - 2j z_{ab} \cos \alpha l \omega} \right]. \quad (69)$$

Using the addition theorems of the trigonometric functions, Eq. (69) can be reduced to

$$Z(\omega) = \frac{1}{j\omega C_o} \left[1 - \frac{2k^2}{\alpha l \omega} \frac{\tan \frac{\alpha l \omega}{2} - j z_{ab}}{1 + z_a z_b - 2j z_{ab} \cot \alpha l \omega} \right]. \quad (70)$$

Therefore, for the admittance, $Y(\omega)$, the following formula is used:

$$Y(\omega) = j\omega C_o \left[1 - \frac{2k^2}{\alpha l \omega} \frac{\tan \frac{\alpha l \omega}{2} - j z_{ab}}{1 + z_a z_b - 2j z_{ab} \cot \alpha l \omega} \right]^{-1}. \quad (71)$$

A. Pure piezoelectric layer

For a single piezoelectric layer without surrounding media (this means $z_a = z_b = z_{ab} = 0$), the series resonance angular frequencies, ω_m^o , are given by the well-known formula [see, e.g., Eq. (9.47) on p. 89 of Tiersten⁴²]

$$1 - \frac{2k^2}{\alpha l \omega_m^o} \tan \frac{\alpha l \omega_m^o}{2} = 0. \quad (72)$$

If $k^2 \ll 1$, then the function $\tan(\alpha l \omega_m^o/2)$ must assume very large values in accordance with Eq. (72) to determine the resonance frequencies, ω_m^o . Consequently, we can write

$$\frac{\alpha l \omega_m^o}{2} = m \frac{\pi}{2} (1 - \delta_m^o), \quad m = 1, 3, 5, \dots \quad (73)$$

with a yet unknown small number $\delta_m^o \ll 1$. Substitution of Eq. (73) into Eq. (72) and taking into account the correction term, δ_m^o , in the tangent function only results in

$$1 = \frac{2k^2}{m\pi} \tan \frac{m\pi}{2} (1 - \delta_m^o). \quad (74)$$

Again, as $\delta_m^o \ll 1$, we can further write

$$\tan \frac{m\pi}{2} (1 - \delta_m^o) = \frac{1}{\tan \frac{m\pi}{2} \delta_m^o} \approx \frac{2}{m\pi \delta_m^o}. \quad (75)$$

And, thus, from Eq. (74), the correction term,

$$\delta_m^o = \frac{4k^2}{m^2 \pi^2}, \quad (76)$$

is obtained to leading order. Therefore, the resonance frequencies, ω_m^o , are approximately given by

$$\omega_m^o = \frac{m\pi}{\alpha l} \left(1 - \frac{4k^2}{m^2 \pi^2} \right), \quad m = 1, 3, 5, \dots \quad (77)$$

B. Resonance circle approximation

To describe the admittance, $Y(\omega) = 1/Z(\omega)$, nearby a resonance frequency, ω_m^o , approximately, one can take the frequency dependencies into account only in the tangent and cotangent functions such that

$$Y_{\text{app}}(\omega) = j\omega_m^o C_o \left[1 - \frac{2k^2}{\alpha l \omega_m^o} \frac{\tan \frac{\alpha l \omega}{2} - j z_{ab}}{1 + z_a z_b - 2j z_{ab} \cot \alpha l \omega} \right]^{-1}. \quad (78)$$

On writing

$$\frac{\alpha l \omega}{2} = m \frac{\pi}{2} + \delta_m \quad \text{with} \quad \delta_m = \frac{\alpha l \omega}{2} - m \frac{\pi}{2}, \quad (79)$$

one obtains

$$\tan \frac{\alpha l \omega}{2} = \tan \left(m \frac{\pi}{2} + \delta_m \right) = -\frac{1}{\tan \delta_m} \quad (80)$$

and

$$\cot \alpha l \omega = \cot(m\pi + 2\delta_m) = \frac{1}{\tan 2\delta_m}. \quad (81)$$

Using the leading order approximation for the tangent function only,

$$\tan \delta_m = \delta_m + O(\delta_m^3), \quad \delta_m \ll 1, \quad (82)$$

a resonance circle approximation is obtained such that

$$Y_{\text{cir}}(\omega) = j\omega_m^o C_o \left[1 - \frac{2k^2}{\alpha l \omega_m^o} \frac{-\frac{1}{\delta_m} - jz_{ab}}{1 + z_a z_b - jz_{ab} \frac{1}{\delta_m}} \right]^{-1} \quad (83)$$

This relation can be rewritten as

$$Y_{\text{cir}}(\omega) = j\omega_m^o C_o \frac{(1 + z_a z_b)\delta_m - jz_{ab}}{(1 + z_a z_b)\delta_m - jz_{ab} + \frac{2k^2}{\alpha l \omega_m^o} (1 + jz_{ab}\delta_m)} \quad (84)$$

Using Eq. (79) results in

$$Y_{\text{cir}}(\omega) = j\omega_m^o C_o \frac{A\omega - B}{C\omega - D}, \quad (85)$$

with the abbreviations

$$A = (1 + z_a z_b) \frac{\alpha l}{2}, \quad (86)$$

$$B = (1 + z_a z_b) \frac{m\pi}{2} + jz_{ab}, \quad (87)$$

$$C = \left(1 + z_a z_b + jz_{ab} \frac{2k^2}{\alpha l \omega_m^o} \right) \frac{\alpha l}{2}, \quad (88)$$

$$D = \left(1 + z_a z_b + jz_{ab} \frac{2k^2}{\alpha l \omega_m^o} \right) \frac{m\pi}{2} + jz_{ab} - \frac{2k^2}{\alpha l \omega_m^o}. \quad (89)$$

The fact that Eq. (85) describes a circle (see Fig. 5) can be deduced from the relation

$$|Y_{\text{cir}}(\omega) - M|^2 = R^2. \quad (90)$$

Here, the center, M , of the circle is given by

$$M = j\omega_m^o C_o \frac{BC^* - AD^*}{C^*D - CD^*}, \quad (91)$$

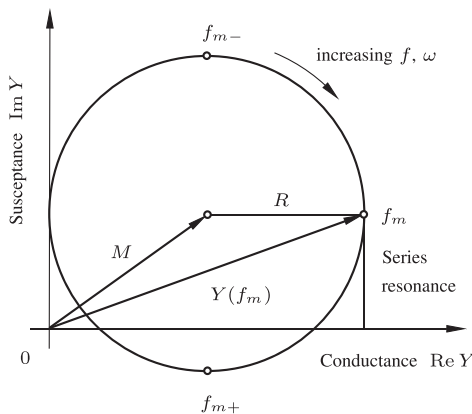


FIG. 5. The circular shape locus of the admittance, $Y(\omega)$, of a piezoelectric resonator in the vicinity of a resonance frequency. The loci of the low impedance characteristic frequencies are also shown. Here, f_{m-} and f_{m+} denote the left and right half value bandwidth frequencies, respectively; f_m is the series resonance frequency (frequency of maximum conductance).

and the radius, R , is given by

$$R = \omega_m^o |C_o| \frac{|AD - BC|}{|C^*D - CD^*|}. \quad (92)$$

Details of the derivation are given in Appendix A.

C. Resonance frequencies

To calculate the series resonance frequency, f_m , and the frequencies, f_{m-} and f_{m+} , necessary for the determination of the half width of the resonance, we use (see Fig. 5)

$$Y_{\text{cir}}(\omega_m) = M + R, \quad (93)$$

$$Y_{\text{cir}}(\omega_{m-}) = M + jR, \quad (94)$$

$$Y_{\text{cir}}(\omega_{m+}) = M - jR. \quad (95)$$

Using Eq. (85), one can write

$$j\omega_m^o C_o \frac{A\omega_m - B}{C\omega_m - D} = M + R \quad (96)$$

or

$$j\omega_m^o C_o (A\omega_m - B) = (C\omega_m - D)(M + R), \quad (97)$$

and, therefore, the resonance angular frequency, ω_m , is given by

$$\omega_m = \frac{j\omega_m^o C_o B - DM - DR}{j\omega_m^o C_o A - CM - CR}. \quad (98)$$

In an analogous way, the angular frequencies, ω_{m-} and ω_{m+} , can be calculated as

$$\omega_{m-} = \frac{j\omega_m^o C_o B - DM - jDR}{j\omega_m^o C_o A - CM - jCR}, \quad (99)$$

$$\omega_{m+} = \frac{j\omega_m^o C_o B - DM + jDR}{j\omega_m^o C_o A - CM + jCR}. \quad (100)$$

Using the explicit expressions for M and R as given in Eqs. (91) and (92), these frequencies are given by (see Appendix B)

$$\omega_m = \frac{D^* \frac{C_o}{|C_o|} + D}{C^* \frac{C_o}{|C_o|} + C} = \frac{D^* \sqrt{C_o} + D \sqrt{C_o^*}}{C^* \sqrt{C_o} + C \sqrt{C_o^*}}, \quad (101)$$

$$\omega_{m-} = \frac{D^* \frac{C_o}{|C_o|} + jD}{C^* \frac{C_o}{|C_o|} + jC} = \frac{D^* \sqrt{C_o} + jD \sqrt{C_o^*}}{C^* \sqrt{C_o} + jC \sqrt{C_o^*}}, \quad (102)$$

$$\omega_{m+} = \frac{D^* \frac{C_o}{|C_o|} - jD}{C^* \frac{C_o}{|C_o|} - jC} = \frac{D^* \sqrt{C_o} - jD \sqrt{C_o^*}}{C^* \sqrt{C_o} - jC \sqrt{C_o^*}}. \quad (103)$$

The half width, $\omega_{m+} - \omega_{m-}$, is given by

$$\omega_{m+} - \omega_{m-} = 2j \frac{DC^* - CD^*}{C^{*2} \frac{C_o}{|C_o|} + C^2 \frac{|C_o|}{C_o}} \quad (104)$$

1. First order approximation for the resonance frequencies

If we consider the common case,

$$z_a \ll 1, \quad z_b \ll 1, \quad k^2 \ll 1, \quad (105)$$

the first order approximations,

$$A = \frac{\alpha l}{2}, \quad B = \frac{m\pi}{2} + jz_{ab}, \quad C = \frac{\alpha l}{2},$$

$$D = \frac{m\pi}{2} + jz_{ab} - \frac{2k^2}{\alpha l \omega_m^o}, \quad (106)$$

and the further approximation (lossless capacitance),

$$\frac{C_o}{|C_o|} \approx 1, \quad (107)$$

this leads to the resonance frequencies,

$$\omega_m = \frac{m\pi - 2 \operatorname{Im} z_{ab} - \frac{4k^2}{|\alpha| l \omega_m^o} \frac{\operatorname{Re} \alpha}{|\alpha|}}{l \operatorname{Re} \alpha}, \quad (108)$$

$$\omega_{m-} = \frac{1}{l(\operatorname{Re} \alpha - \operatorname{Im} \alpha)} \left[m\pi - 2(\operatorname{Re} z_{ab} + \operatorname{Im} z_{ab}) - \frac{4k^2}{|\alpha| l \omega_m^o} \frac{\operatorname{Re} \alpha + \operatorname{Im} \alpha}{|\alpha|} \right], \quad (109)$$

$$\omega_{m+} = \frac{1}{l(\operatorname{Re} \alpha + \operatorname{Im} \alpha)} \left[m\pi + 2(\operatorname{Re} z_{ab} - \operatorname{Im} z_{ab}) - \frac{4k^2}{|\alpha| l \omega_m^o} \frac{\operatorname{Re} \alpha - \operatorname{Im} \alpha}{|\alpha|} \right]. \quad (110)$$

2. Resonance frequency shift

If the resonator is not immersed in a fluid, the resonance frequency is given by

$$\omega_m^o = \frac{m\pi - \frac{4k^2}{|\alpha| l \omega_m^o} \frac{\operatorname{Re} \alpha}{|\alpha|}}{l \operatorname{Re} \alpha}, \quad (111)$$

whereas for the resonator that is in contact with fluids A and B, we obtain

$$\omega_m = \frac{m\pi - 2 \operatorname{Im} z_{ab} - \frac{4k^2}{|\alpha| l \omega_m^o} \frac{\operatorname{Re} \alpha}{|\alpha|}}{l \operatorname{Re} \alpha}. \quad (112)$$

Consequently, the shift of the resonance frequency,

$$\omega_m^o - \omega_m = 2 \frac{\operatorname{Im} z_{ab}}{l \operatorname{Re} \alpha}, \quad (113)$$

depends on the imaginary part of z_{ab} only. Using the relation

$$\alpha z = \rho \quad (114)$$

[see Eqs. (60) and (61)], and taking into account $\operatorname{Im} \alpha \ll \operatorname{Re} \alpha$, we obtain the simple equation,

$$\operatorname{Im} z_{ab} = \frac{l\rho}{2} (\omega_m^o - \omega_m), \quad (115)$$

for the determination of the imaginary part of the acoustic impedances of the fluids A and B.

3. Half width of the resonance

If $\operatorname{Im} \alpha \ll \operatorname{Re} \alpha$, we can use the following simplified expressions:

$$\omega_{m-} = \frac{1}{l \operatorname{Re} \alpha} \left[m\pi - 2(\operatorname{Re} z_{ab} + \operatorname{Im} z_{ab}) - \frac{4k^2}{|\alpha| l \omega_m^o} \frac{\operatorname{Re} \alpha + \operatorname{Im} \alpha}{|\alpha|} \right], \quad (116)$$

$$\omega_{m+} = \frac{1}{l \operatorname{Re} \alpha} \left[m\pi + 2(\operatorname{Re} z_{ab} - \operatorname{Im} z_{ab}) - \frac{4k^2}{|\alpha| l \omega_m^o} \frac{\operatorname{Re} \alpha - \operatorname{Im} \alpha}{|\alpha|} \right], \quad (117)$$

instead of Eqs. (109) and (110) for the calculation of the half width of the resonance. From Eqs. (116) and (117), for the half width, we obtain

$$\omega_{m+} - \omega_{m-} = \frac{4 \operatorname{Re} z_{ab} + \frac{8k^2}{|\alpha| l \omega_m^o} \frac{\operatorname{Im} \alpha}{|\alpha|}}{l \operatorname{Re} \alpha}. \quad (118)$$

Without fluid around the piezoelectric resonator, this half width is determined by the imaginary part of α ,

$$\omega_{m+}^o - \omega_{m-}^o = \frac{8k^2}{l \operatorname{Re} \alpha} \frac{\operatorname{Im} \alpha}{|\alpha|}. \quad (119)$$

Therefore, the change of the half width caused by the fluid is given by

$$(\omega_{m+} - \omega_{m-}) - (\omega_{m+}^o - \omega_{m-}^o) = 4 \frac{\operatorname{Re} z_{ab}}{l \operatorname{Re} \alpha}. \quad (120)$$

As a consequence of Eq. (120), the change of the half width is determined by the real part of z_{ab} . Again, using Eq. (114), one obtains

$$\operatorname{Re} z_{ab} = \frac{l\rho_o}{4} [(\omega_{m+} - \omega_{m-}) - (\omega_{m+}^o - \omega_{m-}^o)] \quad (121)$$

for the determination of the real part of the acoustic impedance of the fluid.

4. Equivalent circuit model

The Butterworth–Van Dyke equivalent circuit model is widely used for the description of the electrical behavior of piezoelectric bulk resonators^{44–46}; see Fig. 6.

Although this circuit model describes the actual resonator in the vicinity of one of its frequencies of resonance only, it has the advantage of being directly applicable to electric circuit analysis. Therefore, it is of great interest to derive the parameters of the equivalent circuit model from our theoretical treatment of piezoelectric resonators.

In many studies, an equivalent circuit diagram for the unloaded resonator is supplemented by further electrical equivalent circuit diagrams for the load.^{47–49} However, here it is shown that for a regarded resonance, the Butterworth–Van Dyke equivalent circuit model is sufficient to describe the entire resonator structure because Eq. (85) describes a circle approximation for the loaded resonator.

The circuit branch, consisting of R_1 , L_1 , and C_1 , is called the motional arm and describes the specific properties of the resonance. Its admittance, $Y_1(\omega)$, is given by

$$Y_1(\omega) = \frac{1}{R_1 + j\omega L_1 + \frac{1}{j\omega C_1}}. \tag{122}$$

It describes a circle with radius $1/(2R_1)$, and the resonance frequencies follow from the relations

$$Y_1(\omega_m) = \frac{1}{R_1}, \tag{123}$$

$$Y_1(\omega_{m-}) = \frac{1+j}{2R_1}, \tag{124}$$

$$Y_1(\omega_{m+}) = \frac{1-j}{2R_1}, \tag{125}$$

with the results

$$\omega_m = \frac{1}{\sqrt{L_1 C_1}}, \tag{126}$$

$$\omega_{m+} - \omega_{m-} = \frac{R_1}{L_1}. \tag{127}$$

Using the circle approximation results given for the circle radius, R , in Eq. (92), the resonance frequency, ω_m , in

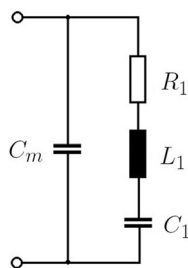


FIG. 6. The Butterworth–Van Dyke equivalent circuit model for one vibration mode of a piezoelectric resonator.

Eqs. (98) or (112), and the half width, $\omega_{m+} - \omega_{m-}$, in Eqs. (104) or (118), we obtain three equations for the calculation of the three elements of the motional arm:

$$R_1 = \frac{1}{2R}, \quad L_1 = \frac{R_1}{\omega_{m+} - \omega_{m-}}, \quad C_1 = \frac{1}{L_1 \omega_m^2}. \tag{128}$$

The parallel capacitance, C_m , is determined by the imaginary part of the center, M , of the circle approximation, which is given in Eq. (91),

$$C_m = \text{Re} \left[C_o \frac{BC^* - AD^*}{C^*D - CD^*} \right]. \tag{129}$$

D. Mechanical displacement

For a piezoelectric layer, Q , without layers, F and G , the mechanical displacement, u_a , given in Eq. (49) can be stated explicitly,

$$u_a = \frac{I_1}{j\omega A} \frac{M^{TD} + j\omega z_B M^{uD}}{M^{Tu} + j\omega z_A M^{TT} + j\omega z_B M^{uu} - \omega^2 z_A z_B M^{uT}}. \tag{130}$$

Using Eqs. (50)–(58) leads to

$$u_a = \frac{I_1}{j\omega A} \sqrt{\frac{1}{\varepsilon \rho}} \frac{-kz(1 - \cos \alpha l \omega) + j\omega z_B \frac{k}{\omega} \sin \alpha l \omega}{-\left(z\omega + \frac{\omega^2 z_A z_B}{z\omega}\right) \sin \alpha l \omega + j\omega(z_A + z_B) \cos \alpha l \omega}.$$

This relation can be written as

$$u_a = \frac{I_1}{j\omega A} \sqrt{\frac{1}{\varepsilon \rho}} kz \frac{1}{z\omega} \frac{1 - \cos \alpha l \omega - jz_b \sin \alpha l \omega}{(1 + z_a z_b) \sin \alpha l \omega - 2jz_{ab} \cos \alpha l \omega}, \tag{131}$$

where the abbreviations are as given in Eqs. (66) and (68). Equation (131) can be simplified to

$$u_a = \frac{I_1}{j\omega A} \sqrt{\frac{1}{\varepsilon \rho}} k \frac{1}{\omega} \frac{1 - \cos \alpha l \omega}{1 + z_a z_b - 2jz_{ab} \cot \alpha l \omega} - jz_b,$$

and can be further simplified to

$$u_a = \frac{I_1}{j\omega A} \sqrt{\frac{1}{\varepsilon \rho}} k \frac{\tan \frac{\alpha l \omega}{2} - jz_b}{\omega (1 + z_a z_b - 2jz_{ab} \cot \alpha l \omega)}. \tag{132}$$

If one has the same fluid on both sides, this means that

$$z_a = z_b = z_{ab}, \tag{133}$$

and we can use the expression from formula (71),

$$\frac{2k^2 \tan \frac{\alpha l \omega}{2} - j z_b}{\alpha l \omega 1 + z_a z_b - 2j z_{ab} \cot \alpha l \omega} = 1 - \frac{j \omega C_o}{Y(\omega)}, \quad (134)$$

to simplify expression (132) even further to obtain

$$u_a = I_1 \frac{\varepsilon}{2e} \left[\frac{1}{j \omega C_o} - \frac{1}{Y(\omega)} \right]. \quad (135)$$

This is a useful short formula for the calculation of the mechanical vibration amplitude. To obtain the maximum value of u_a , the absolute value, $|u_a|$, must be taken as u_a is a function of time.

V. PIEZO-CERAMIC RESONATOR

We consider a 1D resonator structure where the piezo-electric layer of thickness, l , is made of piezoelectric ceramics. If the thickness direction of the piezo-ceramic layer is the direction of the electric polarization of the piezo-ceramic, usually chosen as z -direction, the 8×8 transfer matrix, \mathbf{M}_C , of this layer is given by⁵

$$\mathbf{M}_C = \begin{pmatrix} M_{xx}^{uu} & 0 & 0 & M_{xx}^{uT} & 0 & 0 & 0 & 0 \\ 0 & M_{yy}^{uu} & 0 & 0 & M_{yy}^{uT} & 0 & 0 & 0 \\ 0 & 0 & M_{zz}^{uu} & 0 & 0 & M_{zz}^{uT} & 0 & M_z^{uD} \\ M_{xx}^{Tu} & 0 & 0 & M_{xx}^{TT} & 0 & 0 & 0 & 0 \\ 0 & M_{yy}^{Tu} & 0 & 0 & M_{yy}^{TT} & 0 & 0 & 0 \\ 0 & 0 & M_{zz}^{Tu} & 0 & 0 & M_{zz}^{TT} & 0 & M_z^{TD} \\ 0 & 0 & M_z^{\phi u} & 0 & 0 & M_z^{\phi T} & 1 & M^{\phi D} \\ 0 & 0 & 0 & 0 & 0 & 0 & 0 & 1 \end{pmatrix}. \quad (136)$$

The structure of the transfer matrix implies that an applied electric voltage can only cause mechanical displacement in the z -direction. Therefore, this 8×8 transfer matrix allows a reduction to a 4×4 transfer matrix, whereby the elements of the 4×4 transfer matrix given in Eqs. (50)–(58) have to be calculated with the dielectric constant, ε_{zz} , the elastic constant, c_{zzzz} , and the piezoelectric constant, e_{zzz} .

The material data of the used piezo-ceramic plate resonator PIC255 together with the specific acoustic impedances z of the surrounding media air and water are given in Table I. The thickness, l , was adapted accordingly to include the effect of the electrodes (for the resonator in air, the calculated resonance frequency, f_1 , was adjusted to the experimental resonance frequency) and the imaginary part of the elastic constant, c_{zzzz} , was adjusted to include all of the losses of the experimental setup.

Using these data, we can calculate the admittance, $Y(\omega)$, for all of the frequencies from Eq. (71).

A. Vacuum termination

If the piezo-ceramic resonator is used in vacuum, we have

TABLE I. Material data of the piezo-ceramic resonator PIC255 according to data sheets provided by the manufacturer (PI Ceramic, Lederhose, Germany; see Ref. 55) and the boundary media.

Quantity, symbol	Value	Dimension
Thickness, l	0.892	mm
Piezoelectric active area, A	2.37	cm ²
Density, ρ	7.80	g/cm ³
Elastic constant, c_{zzzz}^E	97.06 + j 0.55	GN/m ²
Dielectric constant, ε_{zz}^S	857.4 - j 17.0	(relative)
Piezoelectric constant, e_{zzz}	13.82	N/(Vm)
Acoustic impedance air, z_{air}	414.0	Ns/m ³
Acoustic impedance water, z_{wat}	1.480 × 10 ⁶	Ns/m ³

$$z_{\text{vacuum}} = 0 \rightarrow z_a = 0, \quad z_b = 0. \quad (137)$$

From Eq. (70), we immediately obtain the well-known result for a piezoelectric plate resonator in vacuum [see, e.g., Eq. (162) on p. 59 of the IEEE Standard on Piezoelectricity³⁷],

$$Z(\omega) = \frac{1}{j \omega C_o} \left[1 - k^2 \frac{\tan \frac{\alpha l \omega}{2}}{\frac{\alpha l \omega}{2}} \right]. \quad (138)$$

B. Air termination

The calculated and measured values of the admittance, $Y(\omega)$, for the frequency range of the first two resonances are shown in Fig. 7 (the measurements were performed using an Agilent 4395A Network/Spectrum/Impedance Analyzer, Agilent Technologies, Inc., Santa Clara, CA). The detailed frequency dependence of the first resonance is depicted in

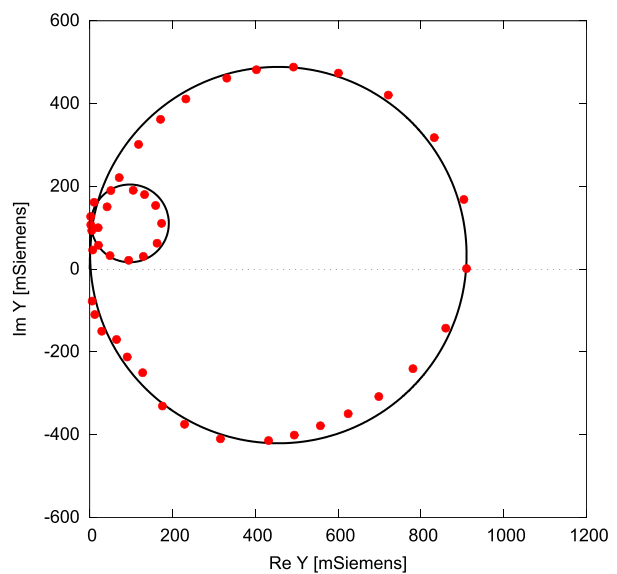


FIG. 7. (Color online) The admittance, $Y(\omega)$, for a piezo-ceramic resonator PIC255 with air at both sides. The first two resonances with resonance frequencies, f_1 and f_3 , are shown [solid line, calculation according to Eq. (68) using the data given in Table I; the dots denote measurement results].

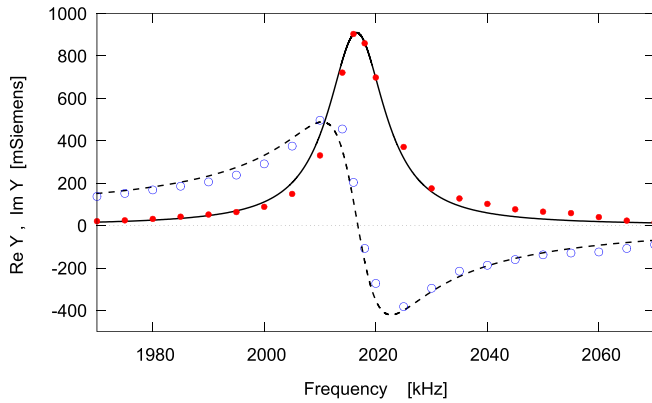


FIG. 8. (Color online) The conductance, $\text{Re} Y(\omega)$, and susceptance, $\text{Im} Y(\omega)$, for a piezo-ceramic resonator PIC255 surrounded by air at both sides (solid line, calculated values for $\text{Re} Y(\omega)$; dashed line, $\text{Im} Y(\omega)$; open and full dots, measurement results). The neighborhood of the first resonance at $f_1 = 2016.6$ kHz is shown.

Fig. 8. The resonance circles become smaller for higher harmonics as can be observed in Fig. 7.

The numerical results for the first two resonance frequencies, f_1 and f_3 , are given in the second column of Table II. Because of the small magnitude of the acoustic impedance of air, there is practically no difference to the results obtained for vacuum.

C. Resonator immersed in water

A significant change in the values of the admittance is obtained when the resonator is immersed in water; see Fig. 9.

In Figs. 10 and 11, the results for air and water surroundings are compared. The shift of the resonance frequencies is vanishingly small, but the half width is drastically changed by the influence of the water surrounding as shown in Fig. 11 and Table II.

D. Mechanical displacement

The mechanical displacement, $u_z(z)$, can be calculated with the help of Eq. (37). The results for an electric current amplitude, $I_1 = 1$ A, are shown in Figs. 12 and 13.

For the air-laden resonator operated at the first resonance frequency $f_1 = 2016.557$ kHz the measured value of the admittance is $Y(\omega_1) = (910 + j34)$ mS, Consequently, the evaluation of Eq. (135) leads to a mechanical vibration amplitude of $u_a = (-0.30 - j10.73)$ nm using the material

TABLE II. Computed resonance frequencies of the piezo-ceramic resonator PIC255 with different outside boundary media.

	Air outside	Water outside	
f_{1-}	2010.398	1939.387	kHz
f_1	2016.557	2016.560	kHz
f_{1+}	2022.720	2094.392	kHz
f_{3-}	6566.626	6502.716	kHz
f_3	6594.103	6594.178	kHz
f_{3+}	6621.581	6685.930	kHz

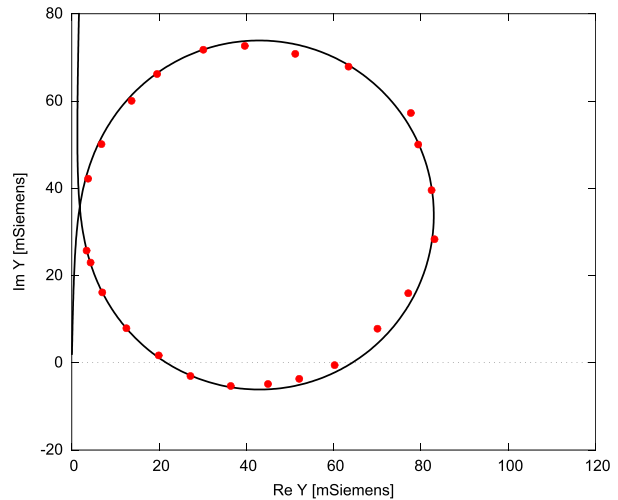


FIG. 9. (Color online) The admittance, $Y(\omega)$, for a piezo-ceramic resonator PIC255 immersed in water at both sides. The neighborhood of the first resonance frequency at $f_1 = 2016.557$ kHz is shown (solid line, calculated values according to Rig-1D-model; dots, measured values).

data given in Table I and an electric current of $I_1 = 1$ A. Its absolute value is $|u_a| = 10.73$ nm, in accordance with the maximum value of u_z shown in Fig. 12.

For the water-laden resonator operated at the first resonance frequency $f_1 = 2016.560$ kHz the measured value of the admittance is $Y(\omega_1) = (84.83 + j26.78)$ mS. Consequently, the evaluation of Eq. (135) leads to a mechanical vibration amplitude of $u_a = (-2.93 - j9.76)$ nm using the material data given in Table I and an electric current of $I_1 = 1$ A. Its absolute value is $|u_a| = 10.2$ nm, in accordance with the maximum value of u_z shown in Fig. 13.

The displacement amplitude for the air-laden resonator is nearly equal to the regarding amplitude of the unladen resonator. In the case of the unladen resonator, $Y(\omega)$ is

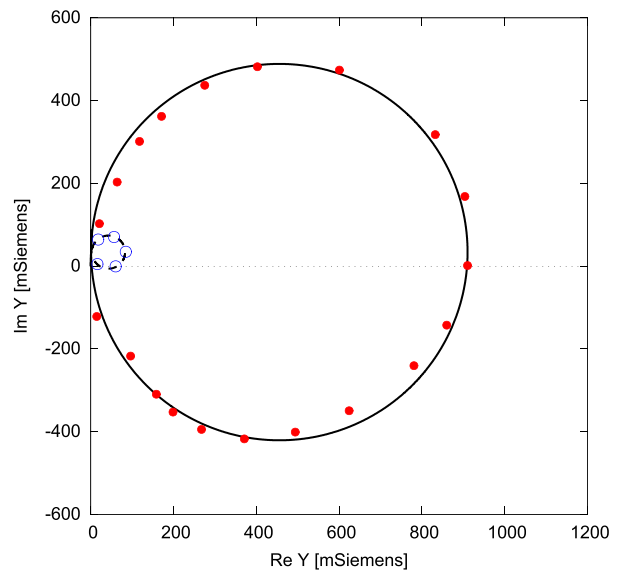


FIG. 10. (Color online) A comparison of the admittance, $Y(\omega)$, for a piezo-ceramic resonator surrounded by air (solid line) and immersed in water (dashed line). The open and solid dots denote measured values. In both cases, only the first resonance is displayed.

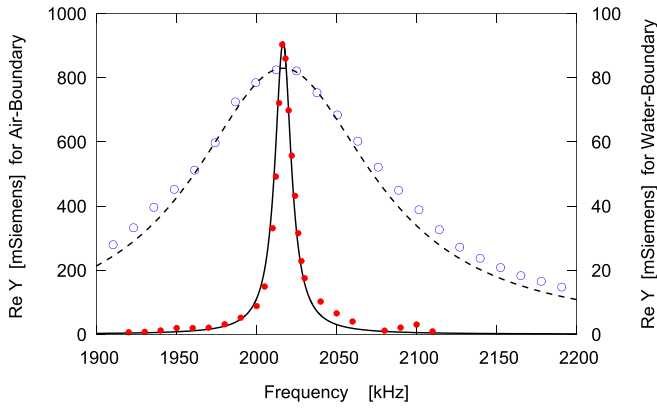


FIG. 11. (Color online) The conductance, $\text{Re } Y(\omega)$, in the neighborhood of the resonance frequency, f_1 , for a piezo-ceramic resonator PIC255 surrounded by air (solid line; scale on the left side) and immersed in water (dashed line; scale on the right side).

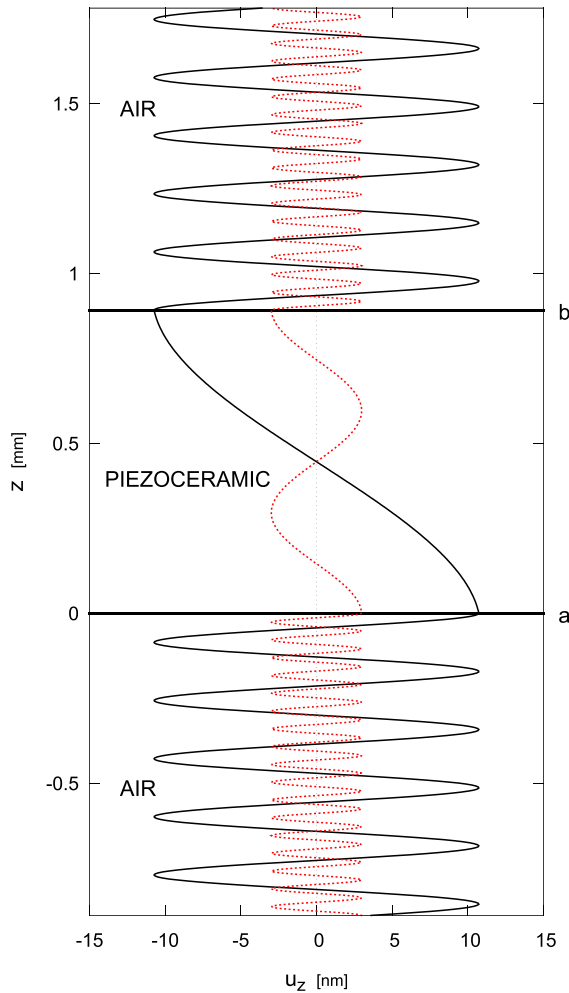


FIG. 12. (Color online) The piezo-ceramic resonator PIC255 of thickness $l = 0.892$ mm in air. The distribution of the longitudinal vibration amplitude, u_z , along the thickness direction, z , is shown for the first resonance (full line) and third resonance (dotted line) for a fixed value of the electric current amplitude, $I_1 = 1$ A. The point in time, t , was chosen such that the maximum amplitude of u_z occurs at $z = 0$, cf. Eq. (143).

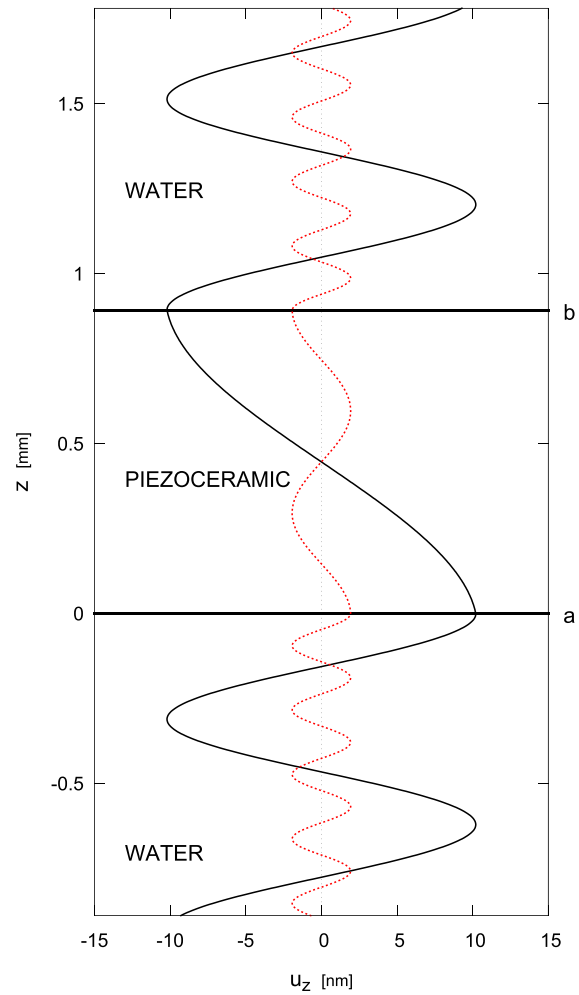


FIG. 13. (Color online) The piezo-ceramic resonator PIC255 of thickness $l = 0.892$ mm immersed in water. The course of the longitudinal vibration amplitude, u_z , along the thickness direction, z , is shown for the first resonance (full line) and third resonance (dotted line) for a fixed value of the electric current amplitude, $I_1 = 1$ A. The point in time, t , was chosen so that the maximum amplitude of u_z occurs at $z = 0$, cf. Eq. (143).

given by the inverse of Eq. (138), which leads to the amplitude, u_a^o , for the unladen resonator,

$$u_a^o = I_1 \frac{\epsilon_{zz}}{2e_{zzz} j \omega C_o} \frac{k^2 \tan \frac{\alpha l \omega}{2}}{\frac{\alpha l \omega}{2}}. \quad (139)$$

This amplitude, u_a^o , can also be calculated from Eq. (132) by setting $z_a = z_b = z_{ab} = 0$, resulting in

$$u_a^o = \frac{I_1}{j \omega A} \sqrt{\frac{1}{\epsilon_{zz} \rho}} \frac{k \tan \frac{\alpha l \omega}{2}}{2}. \quad (140)$$

The numerical evaluation of this formula results in the value $u_a^o = (-0.30 - j 10.73)$ nm. This means that the difference between the regarding results of the unladen and air-laden resonator is extremely small.

E. Restrictions for a linear analysis

The present analysis is based exclusively on the solution of linear equations, cf. the work of Nowotny and Benes.⁵ From a fluid mechanics perspective, however, compression wave phenomena excited in the surrounding fluid allow a solely linear description only under certain restrictions, which are given below. If we assume purely viscous (Newtonian) fluid behavior, the relevant dimensionless groups are the acoustic Mach number, Ma , and the inverse of the acoustic Reynolds number, Re , which is defined by

$$Ma = \frac{|u_a|f}{c_0} \ll 1, \quad \frac{1}{Re} = \frac{\eta}{c_0 \lambda \rho_0} \ll 1, \quad (141)$$

and represent small (perturbation) parameters in the present context. Here, $|u_a|$, f , λ , c_0 , and ρ_0 denote the characteristic wave amplitude, its frequency, wavelength, the sound speed, and density of the fluid, respectively, determined at the quiescent (unperturbed) state. For the acoustic wave in the considered fluid being governed by a linear dissipative wave equation compatible with the approach of the present study, the order of magnitude relations,

$$Ma^2 \ll 1/Re, \quad Ma \gg 1/Re^2, \quad (142)$$

must hold; see, e.g., Ref. 50. In that case, the wave amplitude in the fluid may be approximated by

$$u_z(z, t) = u_a e^{i(\omega t - kz)} e^{-az}, \quad (143)$$

where $k = 2\pi/\lambda$ and the attenuation coefficient a is given by

$$a = \frac{\omega^2 \delta}{2c_0^3}, \quad \delta = \frac{\eta}{\rho_0} \left(\frac{4}{3} + \frac{\zeta}{\eta} + \frac{\gamma - 1}{Pr} \right), \quad (144)$$

see, e.g., Ref. 51 (pp. 225–232). Here, the diffusivity, δ , contains the bulk viscosity, ζ , of the fluid and the last term covers thermal attenuation (neglected in the present study throughout) where γ , $Pr = \eta c_p / \kappa$, c_p , and κ denote the heat capacity ratio, Prandtl number, the specific heat capacity at constant pressure, and thermal conductivity, respectively. For the example presented in Fig. 13 of this study (plane compression wave in water at 20 °C), the reference values are $|u_a| \approx 10^{-8}$ m, $f \approx 2 \times 10^6$ Hz (first resonance frequency), $c_0 \approx 1440$ m/s, $\rho_0 \approx 998$ kg/m³, $\eta \approx 10^{-3}$ Pa s, and $\lambda = c_0/f \approx 0.7 \times 10^{-3}$ m. As a consequence, we obtain $Ma \approx 10^{-5}$ and $1/Re \approx 10^{-3}$, which is in full agreement with the conditions (142) of linear acoustics.

Based on the water data given in Thompson,⁵¹ one finds $4/3 + \zeta/\eta \approx 4.4$ and $(\gamma - 1)/Pr \approx 0.93 \times 10^{-3}$, indicating that the propagation of a compression wave in water (or, in general, in liquids in contrast to the situation with gases) can be viewed as an isothermal process in very good approximation. The diffusivity is $\delta \approx 4.4 \times 10^{-6}$ m²/s, and for the attenuation coefficient, one obtains $a \approx 0.12$ m⁻¹ for our example.

VI. AT-CUT QUARTZ RESONATOR

We consider a resonator structure where the piezoelectric layer is an AT-cut quartz.³⁷ The thickness direction is chosen to be the y -direction. Then, the general 8×8 transfer matrix, \mathbf{M}_Q , of the quartz layer is given by

$$\mathbf{M}_Q = \begin{pmatrix} M_{xx}^{uu} & 0 & 0 & M_{xx}^{uT} & 0 & 0 & 0 & M_x^{uD} \\ 0 & M_{yy}^{uu} & 0 & 0 & M_{yy}^{uT} & 0 & 0 & 0 \\ 0 & 0 & M_{zz}^{uu} & 0 & 0 & M_{zz}^{uT} & 0 & 0 \\ M_{xx}^{Tu} & 0 & 0 & M_{xx}^{TT} & 0 & 0 & 0 & M_x^{TD} \\ 0 & M_{yy}^{Tu} & 0 & 0 & M_{yy}^{TT} & 0 & 0 & 0 \\ 0 & 0 & M_{zz}^{Tu} & 0 & 0 & M_{zz}^{TT} & 0 & 0 \\ M_x^{\phi u} & 0 & 0 & M_x^{\phi T} & 0 & 0 & 1 & M^{\phi D} \\ 0 & 0 & 0 & 0 & 0 & 0 & 0 & 1 \end{pmatrix}. \quad (145)$$

The structure of the transfer matrix implies that an electric voltage applied to the electrodes can only cause mechanical displacement in the x -direction and, consequently, a purely transversal wave (thickness shear mode) is excited. Therefore, this 8×8 transfer matrix allows a reduction to a 4×4 transfer matrix, whereby the elements of the 4×4 transfer matrix given in Eqs. (50)–(58) have to be calculated with the dielectric constant, ϵ_{yy} , elastic constant, c_{yyxx} , and piezoelectric constant, e_{yyx} .

Calculations based on the Rig-1D-model and regarding measurements have been performed for an AT-cut quartz resonator manufactured by KRYSTALY (Hradec Králové, Czech Republic). The data of this resonator are given in Table III. The thickness of the AT-cut plate (including the electrodes) was adjusted such that the calculation fits the measured resonance frequency, f_1 , and the imaginary part of the elastic constant was tuned accordingly to include all of the losses. Using these data, we can calculate the admittance, $Y(\omega)$, for all of the frequencies from Eq. (71).

A. Boundary medium air

Figure 14 depicts the measured and calculated admittances, $Y(\omega)$. The frequency dependencies of the conductance, $\text{Re} Y(\omega)$, and susceptance, $\text{Im} Y(\omega)$, are depicted in Fig. 15.

TABLE III. Material data of the AT-cut quartz resonator according to data sheets provided by the manufacturer (KRYSTALY, Hradec Králové, Czech Republic; see Ref. 56; model 1, shape plano-convex).

Quantity, symbol	Value	Dimension
Thickness, l	0.334451	mm
Piezoelectric active area, A	0.135	cm ²
Density, ρ_Q	2.649	g/cm ³
Elastic constant, c_{yyxx}^E	$29.01 + j0.00045$	GN/m ²
Dielectric constant, ϵ_{yy}^S	$4.50 - j0.0045$	(Relative)
Piezoelectric constant, e_{yyx}	-0.095	N/(Vm)

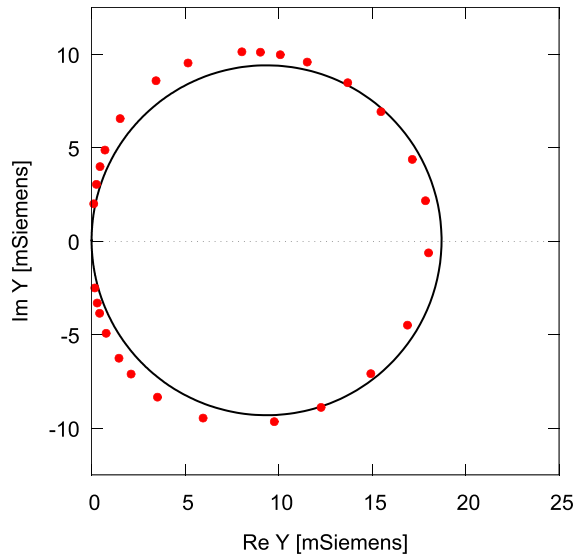


FIG. 14. (Color online) The admittance, $Y(\omega)$, for an AT-cut quartz resonator surrounded by air on both sides. The first resonance with frequency $f_1^0 = 4950.953$ kHz is depicted in the figure [solid line denotes results according to Eq. (71) using the data given in Table III, and the dots denote experimental results].

The resonance frequencies, f_1 , f_{1+} , and f_{1-} are determined from these curves and given in Table V. The calculation was performed according to Eq. (71) with the data given in Table III and by using $z_{ab} = 0$ because the difference of $Y(\omega)$ between vacuum and air is too small to appear in Figs. 14 and 15.

B. Boundary medium oil

Measurements were also carried out with viscosity standard oil S200 surrounding the AT-cut quartz resonator at a temperature of 30 °C. The data of this standard oil are given in Table IV.

A significant change of the admittance values is observed when both sides of the resonator are brought into contact with the oil S200; see Figs. 16 and 17. Here, the

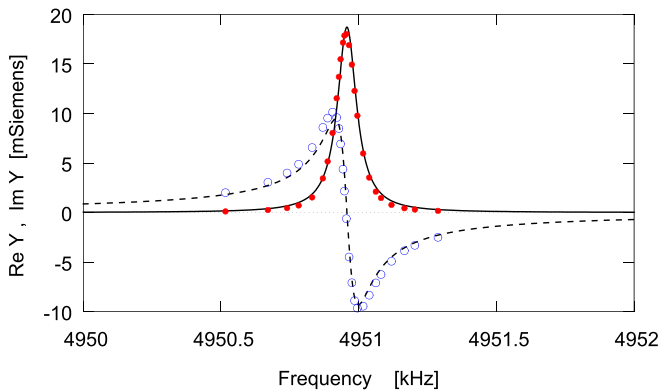


FIG. 15. (Color online) The conductance, $\text{Re} Y(\omega)$, and susceptance, $\text{Im} Y(\omega)$, for an AT-cut quartz resonator surrounded by air on both sides (solid line denotes calculated values for $\text{Re} Y(\omega)$, dashed line denotes $\text{Im} Y(\omega)$, and open and full dots denote experimental results). The neighborhood of the first resonance at $f_1^0 = 4950.953$ kHz is depicted in the graph.

TABLE IV. Certified viscosity oil standard S200 in accordance with ASTM D2162 and ASTM D1480.

Temperature (°C)	Viscosity η (mPa s)	Density ρ (g/cm ³)
20.00	447.0	0.8395
25.00	331.6	0.8365
37.78	166.5	0.8287
40.00	149.3	0.8274

maximum value of $\text{Re} Y(\omega)$ is about 400 times smaller compared to the unladen case. Furthermore, the resonance frequency is shifted accordingly as shown in Table V, where the first mode resonance frequencies are listed.

These frequencies can be used to calculate the acoustic impedance, z_L , of standard oil S200 from Eqs. (118) and (114) such that

$$z_L \approx (60.0 + j59.0) \text{ kNs/m}^3. \quad (146)$$

As the real and imaginary parts of the acoustic impedance are nearly equal, the oil S200 can be considered as a Newtonian fluid under the given circumstances. From the acoustic impedance given in Eq. (146), one obtains the viscosity of oil S200 as

$$\eta_L \approx 276 \text{ mPa s}. \quad (147)$$

Thereby we used the density,

$$\rho_L \approx 834 \text{ kg/m}^3, \quad (148)$$

which is obtained from Table IV by interpolation.

Figure 18 illustrates that the resonance frequency shift is half the broadening of the resonance curve for oil S200, and f_1^{air} is nearly equal to f_1^{oil} . This is a good confirmation of

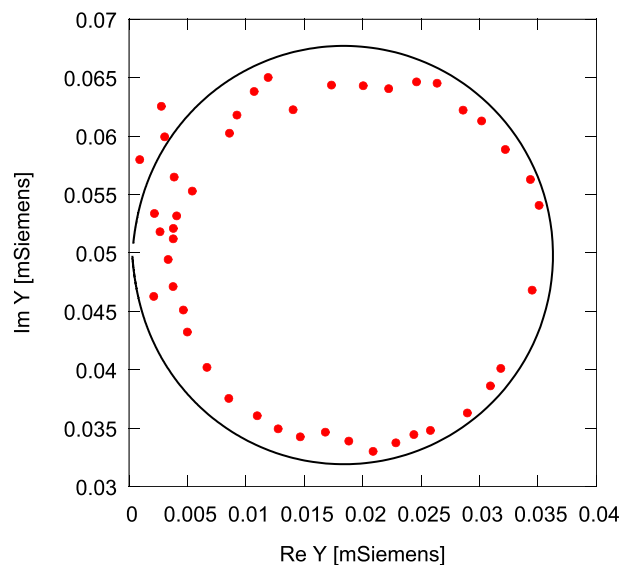


FIG. 16. (Color online) The admittance, $Y(\omega)$, for an AT-cut quartz resonator with standard oil S200 at both sides. The neighborhood of the first resonance frequency at $f_1^t = 4929$ kHz is displayed (solid line denotes calculated values, and dots denote measured values).

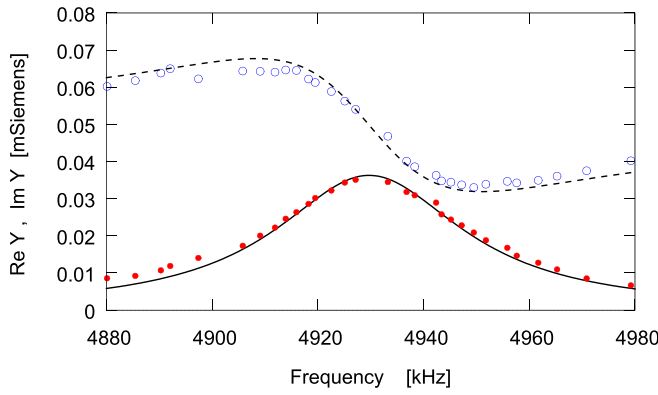


FIG. 17. (Color online) The conductance, $\text{Re} Y(\omega)$, and susceptance, $\text{Im} Y(\omega)$, for an AT-cut quartz resonator in contact with standard oil S200 at both sides (solid line denotes calculated values for $\text{Re} Y(\omega)$, dashed line denotes $\text{Im} Y(\omega)$, and open and full dots denote experimental results). The neighborhood of the first resonance at $f_1^L = 4929$ kHz is depicted in the graph.

the results given in Eqs. (133) and (134) for the resonance frequency shift and enlargement of the half width. All of the calculations for the AT-cut quartz resonator in oil S200 were performed with the acoustic impedance given in Eq. (146).

C. Fluid at one side of the resonator only

For a piezoelectric resonator with a fluid medium A only on one side, we have

$$z_{ab} = \frac{z_a}{2}, \quad (149)$$

and, therefore, from Eqs. (113) and (120),

$$\omega_m^o - \omega_m = \frac{\text{Im} z_a}{l \text{Re} \alpha}, \quad (150)$$

$$(\omega_{m+} - \omega_{m-}) - (\omega_{m+}^o - \omega_{m-}^o) = 2 \frac{\text{Re} z_a}{l \text{Re} \alpha}. \quad (151)$$

Using Eq. (73) in the approximate form,

$$l \text{Re} \alpha = \frac{m \pi}{\omega_m^o}, \quad m = 1, 3, 5, \dots, \quad (152)$$

one can write

$$\omega_m^o - \omega_m = \frac{\omega_m^o}{m \pi} \text{Im} z_a, \quad (153)$$

$$(\omega_{m+} - \omega_{m-}) - (\omega_{m+}^o - \omega_{m-}^o) = 2 \frac{\omega_m^o}{m \pi} \text{Re} z_a. \quad (154)$$

TABLE V. Measured resonance frequencies of the AT-cut quartz resonator with different surrounding media.

	Outside air	Outside oil S200	
f_{1-}	4950.907	4907	kHz
f_1	4950.953	4929	kHz
f_{1+}	4951.002	4952	kHz

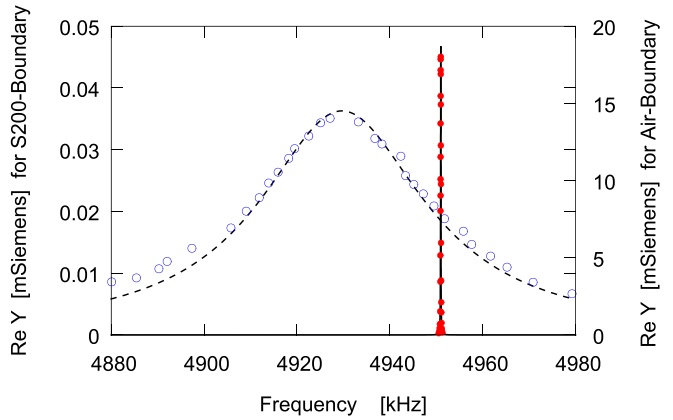


FIG. 18. (Color online) A comparison of the conductance, $\text{Re} Y(\omega)$, of an AT-cut quartz resonator with surrounding air (scale on the right side) and oil S200 (scale on the left side) (solid line denotes calculated values for oil, dashed line denotes calculated values for air, and full and open dots denote the respective measured values). In both cases, only the first resonance is shown.

Using the viscosity, η_A and the density, ρ_A , of the fluid A , the specific acoustic impedance, z_A , is given by

$$z_A = \sqrt{j\omega \eta_A \rho_A}. \quad (155)$$

Together with the specific acoustic impedance, z , given in Eq. (61), one obtains

$$z_a = \frac{z_A}{z} = \sqrt{\frac{j\omega \eta_A \rho_A}{\bar{c} \rho}}. \quad (156)$$

For a Newtonian fluid, the real and imaginary parts of z_a are equal:

$$\text{Re} z_a = \text{Im} z_a = \sqrt{\frac{\omega \eta_A \rho_A}{2 \bar{c} \rho}}. \quad (157)$$

On the right sides of Eqs. (153), (154), and (157), always choosing ω_m for ω_m^o and ω , one can write

$$\omega_m^o - \omega_m = \frac{\omega_m}{m \pi} \sqrt{\frac{\omega_m \eta_A \rho_A}{2 \bar{c} \rho}}, \quad (158)$$

$$(\omega_{m+} - \omega_{m-}) - (\omega_{m+}^o - \omega_{m-}^o) = 2 \frac{\omega_m}{m \pi} \sqrt{\frac{\omega_m \eta_A \rho_A}{2 \bar{c} \rho}}. \quad (159)$$

Furthermore, by using $\omega_m = 2\pi f_m$ in Eq. (158), one obtains the well-known formula for the resonance frequency shift caused by a Newtonian fluid (see, e.g., Refs. 5, 32, and 52),

$$f_m - f_m^o = -\frac{f_m^{3/2}}{m} \sqrt{\frac{\eta_A \rho_A}{\pi \bar{c} \rho}}. \quad (160)$$

Finally, the change of the frequency half width can be obtained from Eq. (159) to give

$$(f_{m+} - f_{m-}) - (f_{m+}^o - f_{m-}^o) = 2 \frac{f_m^{3/2}}{m} \sqrt{\frac{\eta_A \rho_A}{\pi \bar{c} \rho}}. \quad (161)$$

Therefore, for a Newtonian fluid, the change of the frequency half width is twice the shift of the resonance frequency. If the determination of η_A from Eqs. (160) and (161) results in different values, the fluid exhibits a non-Newtonian behavior and, consequently, one has to use the more general formulas given by Eqs. (153) and (154).

D. Accuracy of the used approximations

To obtain an impression of the accuracy of the approximations used in Eq. (71) in the form of Eqs. (101)–(103) and, further, Eqs. (108)–(110), the regarded calculated numerical values of the frequencies are given in Table VI. From Eq. (71), one cannot compute the resonance frequencies in a direct way, and only the function $Y(\omega)$ can be calculated and, therefore, we have to search for the extremes. The values listed in Table VI confirm that in the case of surrounding air, the different approximation steps result in equal values, whereas in the case of surrounding oil S200, the differences between the results are very small compared to the considerable shift of the frequencies from surrounding air to surrounding oil S200. Consequently, the calculation of the resonance frequencies (and, in a further step, the determination of the viscosity of the fluid) can be performed with sufficient accuracy by using Eqs. (108)–(110).

E. Mechanical displacement

The mechanical displacement, $u_x(y, t)$, can be calculated with the help of formula Eq. (37). The result for an electric current amplitude, $I_1 = 1$ mA, is depicted in Fig. 19. For the oil-laden resonator operated at the first resonance frequency $f_1 = 4929$ kHz, the measured value of the admittance is $Y(\omega_1) = (0.035 + j0.050)$ mS Using the material data given in Table III and an electric current of $I_1 = 1$ mA, a value of $u_a = (1.97 + j 1.40)$ nm for the mechanical vibration amplitude is obtained. The maximum amplitude is, thus, $|u_a| = 2.42$ nm, which is in agreement with the results depicted in Fig. 19.

An analogous calculation for the air-laden resonator operated at the first resonance frequency $f_1 = 4950.95$ kHz with a measured value of the admittance $Y(\omega_1) = (18.7 + j0.05)$ mS, and an electric current of $I_1 = 1$ mA, gives the mechanical amplitude $u_a = (0.01 + j4.19)$ nm. The

TABLE VI. Calculated resonance frequencies of the AT-cut quartz resonator using the exact result, Eq. (71), and the approximations, Eqs. (101)–(103) and (108)–(110).

	Equation (71)	Equations (101)–(103)	Equations (108)–(110)	
Air outside				
f_{1-}^o	4950.915	4950.915	4950.915	kHz
f_1^o	4950.957	4950.957	4950.957	kHz
f_{1+}^o	4950.999	4950.999	4950.999	kHz
Oil S200 outside				
f_{1-}	4908.288	4908.131	4908.140	kHz
f_1	4929.694	4929.748	4929.749	kHz
f_{1+}	4951.102	4951.339	4951.337	kHz

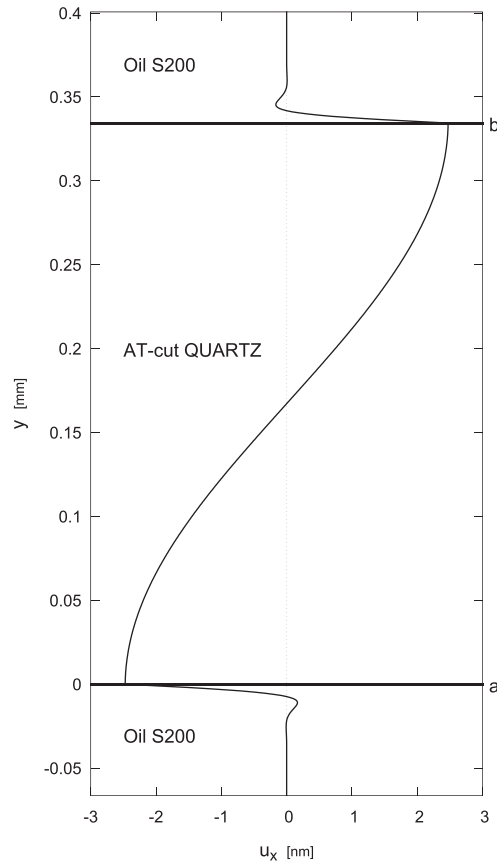


FIG. 19. An AT-cut quartz resonator of thickness $l = 0.334451$ mm in standard oil S200. The course of the transversal vibration amplitude, u_x , along the thickness direction, y , is shown for the first resonance frequency, $f_1 = 4929$ kHz, for an electric current amplitude of $I_1 = 1$ mA. The point in time, t , was chosen such that the maximum amplitude of u_x occurs at $y = 0$, cf. Eq. (165).

maximum amplitude is, thus, $|u_a| = 4.19$ nm. Consequently, the oil causes a reduction of the mechanical vibration amplitude of about 40%.

In the case of the unladen resonator, we can use Eq. (132) with $z_a = z_b = z_{ab} = 0$ such that

$$u_a^o = \frac{I_1}{j\omega A} \sqrt{\frac{1}{\epsilon\rho} \frac{k}{\omega}} \tan \frac{\alpha l \omega}{2}. \tag{162}$$

The numerical evaluation of this formula results in the value $u_a^o = (0.01 + j4.19)$ nm. This means that the difference in displacement amplitudes between the unladen and air-laden resonator is extremely low.

For a Newtonian fluid A with the shear (dynamic) viscosity, η_A , the acoustic impedance, z_A , and slowness, α_A , are given by

$$z_A = \sqrt{j\omega\eta_A\rho_A}, \quad \alpha_A = \frac{1-j}{\sqrt{2}} \sqrt{\frac{\rho_A}{\omega\eta_A}}, \tag{163}$$

and the displacement course, $u_x(y, t)$, of the strongly damped shear wave in the fluid (see Fig. 19) with the characteristic penetration depth,

$$\delta_A = \sqrt{2\eta_A/(\omega\rho_A)}, \tag{164}$$

is given by

$$u_x(y, t) = u_a e^{j(\omega t - y/\delta_A)} e^{-y/\delta_A}, \tag{165}$$

which is in full agreement with the situation in the so-called Stokes oscillating boundary layer (or Stokes second problem); see, e.g., the chapter entitled ‘‘Oscillatory motion in a viscous fluid’’ on pp. 83–92 in Ref. 53. Most importantly, here, the amplitude of the shear wave according to Eq. (37) can be stated explicitly, cf. the study of Jakoby.⁵⁴

VII. SUMMARY AND CONCLUSIONS

A general transfer matrix description for 1D layered structures consisting of piezoelectric and non-piezoelectric layers of arbitrary number and with termination layers of arbitrary acoustic impedance has been introduced and applied to calculate the frequency-dependent electrical admittance between two electrodes. Furthermore, explicit formulas for the computation of the spatial dependence along the normal axis of the quantities displacement, \vec{u} , strain, \vec{T} , electric potential, φ , and dielectric displacement, D_ν , have been derived. For the spatial course of the displacement characteristic, numerical examples have been presented for longitudinal waves generated by a typical piezo-ceramic and shear-waves generated by an AT-cut quartz plate. From these examples, it can be learned that the mechanical amplitude is directly proportional to the electric driving voltage, and the proportionality factor is determined by the electric admittance, piezoelectric constant, and dielectric constant. Thus, the hardly measurable mechanical vibration amplitudes can be computed simply from the easy to measure driving voltage and electric admittance.

A comparison between model predictions and measurements shows good agreement for the resonance frequency shift and broadening of the conductance resonance curve—in particular, the increase in the full width at half-maximum (FWHM)—caused by the boundary medium. Moreover, useful analytical expressions for the determination of the mechanical displacement amplitudes of the fluid-laden and unladen resonators are presented and used for calculating the spatial course of these vibration amplitudes for the investigated exemplary samples.

The main results for fluid viscosity sensors are Eqs. (115) and (121), which show that the shift of the resonance frequency caused by the fluid is connected to the imaginary part of the acoustic impedance of the fluid, whereas the broadening of the conductance resonance curve, in particular, the FWHM, is related to its real part. In the case of a Newtonian fluid, the shift of the resonance frequency or FWHM of the conductance resonance curve can be used to calculate the shear viscosity of the fluid in contact with the piezoelectric resonator.

ACKNOWLEDGMENTS

This work was supported by the European Commission within the GROWTH shared cost RTD funding scheme, QxSens Project No. GRD1-2001-41816. Open access funding provided by Technische Universität Wien Bibliothek.

APPENDIX A: CIRCLE EQUATION

Substituting Eq. (85) into Eq. (90) results in

$$\left| j\omega_m^o C_o \frac{A\omega - B}{C\omega - D} - M \right|^2 = R^2. \tag{A1}$$

Using

$$M = j\omega_m^o C_o \frac{BC^* - AD^*}{C^*D - CD^*} \tag{A2}$$

and

$$R = \omega_m^o |C_o| \frac{|AD - BC|}{|C^*D - CD^*|}, \tag{A3}$$

one can write

$$\left| \frac{A\omega - B}{C\omega - D} - \frac{BC^* - AD^*}{C^*D - CD^*} \right|^2 = \frac{|AD - BC|^2}{|C^*D - CD^*|^2}. \tag{A4}$$

With

$$\begin{aligned} & \frac{A\omega - B}{C\omega - D} - \frac{BC^* - AD^*}{C^*D - CD^*} \\ &= \frac{(A\omega - B)(C^*D - CD^*) - (C\omega - D)(BC^* - AD^*)}{(C\omega - D)(C^*D - CD^*)} \\ &= \frac{(AC^*D - CBC^*)\omega + (BCD^* - DAD^*)}{(C\omega - D)(C^*D - CD^*)} \\ &= \frac{(AD - CB)(C^*\omega - D^*)}{(C\omega - D)(C^*D - CD^*)} \end{aligned} \tag{A5}$$

and

$$\left| \frac{C^*\omega - D^*}{C\omega - D} \right|^2 = 1, \tag{A6}$$

one can see that Eq. (A4) is fulfilled and, therefore, Eq. (85), in fact, represents a circle.

APPENDIX B: FREQUENCY CALCULATION

Using

$$\begin{aligned} & j\omega_m^o C_o B - DM \\ &= j\omega_m^o C_o \left(B - D \frac{BC^* - AD^*}{C^*D - CD^*} \right) \\ &= j\omega_m^o C_o \frac{BC^*D - BCD^* - DBC^* + DAD^*}{C^*D - CD^*} \\ &= j\omega_m^o C_o D^* \frac{AD - BC}{C^*D - CD^*} \end{aligned} \tag{B1}$$

and

$$\begin{aligned} j\omega_m^o C_o A - CM &= j\omega_m^o C_o \left(A - C \frac{BC^* - AD^*}{C^*D - CD^*} \right) \\ &= j\omega_m^o C_o \frac{AC^*D - ACD^* - CBC^* + CAD^*}{C^*D - CD^*} \\ &= j\omega_m^o C_o C^* \frac{AD - BC}{C^*D - CD^*}, \end{aligned} \quad (B2)$$

from Eq. (98), one obtains

$$\omega_m = \frac{j\omega_m^o C_o D^* (AD - BC) - DR(C^*D - CD^*)}{j\omega_m^o C_o C^* (AD - BC) - CR(C^*D - CD^*)}. \quad (B3)$$

Using the expression for R given in Eq. (92), one can write

$$\omega_m = \frac{j\omega_m^o C_o D^* F_A - DF_C \omega_m^o |C_o| \frac{|F_A|}{|F_C|}}{j\omega_m^o C_o C^* F_A - CF_C \omega_m^o |C_o| \frac{|F_A|}{|F_C|}}, \quad (B4)$$

with the factors $F_A = AD - BC$ and $F_C = C^*D - CD^*$. Explicitly, one can write

$$\omega_m = \frac{D^* \frac{C_o}{|C_o|} \frac{AD - BC}{|AD - BC|} + jD \frac{C^*D - CD^*}{|C^*D - CD^*|}}{C^* \frac{C_o}{|C_o|} \frac{AD - BC}{|AD - BC|} + jC \frac{C^*D - CD^*}{|C^*D - CD^*|}}. \quad (B5)$$

By using Eqs. (86)–(89), the calculation of the factor, F_A , gives a simple result:

$$\begin{aligned} F_A &= (1 + z_a z_b) \frac{\alpha l}{2} \\ &\times \left[\left(1 + z_a z_b + jz_{ab} \frac{2k^2}{\alpha l \omega_m^o} \right) \frac{m\pi}{2} + jz_{ab} - \frac{2k^2}{\alpha l \omega_m^o} \right] \\ &- \left[(1 + z_a z_b) \frac{m\pi}{2} + jz_{ab} \right] \left[1 + z_a z_b + jz_{ab} \frac{2k^2}{\alpha l \omega_m^o} \right] \frac{\alpha l}{2} \\ &= (1 + z_a z_b) \frac{\alpha l}{2} \left[jz_{ab} - \frac{2k^2}{\alpha l \omega_m^o} \right] \\ &- jz_{ab} \left[1 + z_a z_b + jz_{ab} \frac{2k^2}{\alpha l \omega_m^o} \right] \frac{\alpha l}{2} \\ &= -(1 + z_a z_b) \frac{\alpha l}{2} \frac{2k^2}{\alpha l \omega_m^o} + z_a z_b \frac{2k^2}{\alpha l \omega_m^o} \frac{\alpha l}{2} = -\frac{k^2}{\omega_m^o}. \end{aligned} \quad (B6)$$

Consequently, one obtains

$$\frac{AD - BC}{|AD - BC|} = -1. \quad (B7)$$

Furthermore, $C^*D - CD^*$ is purely imaginary,

$$\frac{C^*D - CD^*}{|C^*D - CD^*|} = j. \quad (B8)$$

Using Eqs. (B7) and (B8), formula (B5) for the resonance frequency can be written as

$$\omega_m = \frac{D^* \frac{C_o}{|C_o|} + D}{C^* \frac{C_o}{|C_o|} + C}. \quad (B9)$$

In an analogous manner, one obtains

$$\omega_{m-} = \frac{D^* \frac{C_o}{|C_o|} + jD}{C^* \frac{C_o}{|C_o|} + jC} \quad (B10)$$

and

$$\omega_{m+} = \frac{D^* \frac{C_o}{|C_o|} - jD}{C^* \frac{C_o}{|C_o|} - jC}. \quad (B11)$$

¹R. A. Crane and G. Fischer, "Analysis of a quartz crystal microbalance with coatings of finite viscosity," *J. Phys. D: Appl. Phys.* **12**, 2019–2026 (1979).
²A. Ballato, "Piezoelectric resonators loaded with viscoelastic and nonuniform media," in *Proceedings of the 2002 IEEE International Frequency Control Symposium and PDA Exhibition 2002* (2002), pp. 191–201.
³I. D. Avramov, "Analysis and design of negative resistance oscillators using surface transverse wave-based single port resonators," *IEEE Trans. Ultrason., Ferroelectr., Freq. Control* **50**(3), 220–229 (2003).
⁴A. Ballato, "Mems fluid viscosity sensor," *IEEE Trans. Ultrason., Ferroelectr., Freq. Control* **57**(3), 669–676 (2010).
⁵H. Nowotny and E. Benes, "General one-dimensional treatment of the layered piezoelectric resonator with two electrodes," *J. Acoust. Soc. Am.* **82**(2), 513–521 (1987).
⁶H. Nowotny, E. Benes, and M. Schmid, "Layered piezoelectric resonators with an arbitrary number of electrodes (general one-dimensional treatment)," *J. Acoust. Soc. Am.* **90**(3), 1238–1245 (1991).
⁷S. Radel and E. Benes, "Utilisation of layered piezoelectric resonators for the online measurement of mass density and viscosity of fluids," *Elektrotech. Informationstech.* **126**, 19–30 (2009).
⁸S. P. Martin, R. J. Townsend, L. A. Kuznetsova, K. A. Borthwicka, M. Hill, M. B. McDonnell, and W. T. Coakley, "Spore and micro-particle capture on an immunosensor surface in an ultrasound standing wave system," *Biosens. Bioelectron.* **21**(5), 758–767 (2005).
⁹T. Schwarz and J. Dual, "Ultrasonic resonator for manipulation of bacteria," *AIP Conf. Proc.* **1433**(1), 779–782 (2012).
¹⁰B. Sveshnikov, "Universal modeling of the bulk acoustic wave devices," in *2009 IEEE International Frequency Control Symposium Joint with the 22nd European Frequency and Time Forum* (2009), pp. 466–469.
¹¹G. Wingqvist, V. Yantchev, and I. Katardjiev, "Mass sensitivity of multi-layer thin film resonant BAW sensors," *Sens. Actuators, A* **148**(1), 88–95 (2008).
¹²M. Moreira, J. Bjurström, I. Katardjiev, and V. Yantchev, "Aluminum scandium nitride thin-film bulk acoustic resonators for wide band applications," *Vacuum* **86**(1), 23–26 (2011).
¹³R. Milsom, H.-P. Lobl, C. Metzmacher, P. Lok, A. Tuinhout, and F. van Straten, "2D model of solidly-mounted and membrane BAW devices," in *IEEE Symposium on Ultrasonics 2003* (2003), Vol. 2, pp. 1802–1807.
¹⁴R. Ohara, K. Sano, N. Yanase, T. Yasumoto, T. Kawakubo, and K. Itaya, "High- q thin film bulk acoustic wave resonator using highly (111)-"

- oriented aluminum electrode,” in *Proceedings - IEEE Ultrasonics Symposium* (2005), Vol. 1, pp. 206–209.
- ¹⁵A. Reinhardt, S. Ballandras, and V. Laude, “Simulation of transverse effects in FBAR devices,” in *IEEE MTT-S International Microwave Symposium Digest* (2005), pp. 237–240.
- ¹⁶C. C. W. Ruppel, “Acoustic wave filter technology—A review,” *IEEE Trans. Ultrason., Ferroelect., Freq. Control* **64**(9), 1390–1400 (2017).
- ¹⁷M. Y. Dvoesherstov and V. I. Cherednik, “Microwave bandpass filters based on thin-film acoustic resonators: Theory and experiment,” *Acoust. Phys.* **61**(6), 657–664 (2015).
- ¹⁸J. Bjurström, “Advanced thin film electroacoustic devices,” Doctoral thesis, Uppsala University, Uppsala, Sweden, 2007, available at <http://urn.kb.se/resolve?urn=urn%3Anbn%3Ase%3Auu%3Adiva-7672>.
- ¹⁹S. Oberti, A. Neild, and J. Dual, “Manipulation of micrometer sized particles within a micromachined fluidic device to form two-dimensional patterns using ultrasound,” *J. Acoust. Soc. Am.* **121**(2), 778–785 (2007).
- ²⁰R. Barnkob, P. Augustsson, T. Laurell, and H. Bruus, “Measuring the local pressure amplitude in microchannel acoustophoresis,” *Lab Chip* **10**(5), 563–570 (2010).
- ²¹R. Krimholtz, D. A. Leedom, and G. L. Matthaei, “New equivalent circuits for elementary piezoelectric transducers,” *Electron. Lett.* **6**, 398–399 (1970).
- ²²M. Dvoesherstov, V. Cherednik, S. Bosov, I. Orlov, and O. Rudenko, “Numerical and experimental analysis of the parameters of an electroacoustic thin-film microwave resonator,” *Acoust. Phys.* **59**(5), 513–520 (2013).
- ²³G. Behling, R. Lucklum, and P. Hauptmann, “Fast three-step method for shear moduli calculation from quartz crystal resonator measurements,” *IEEE Trans. Ultrason., Ferroelect., Freq. Control* **46**(6), 1431–1438 (1999).
- ²⁴R. Behrends and U. Kaatze, “A high frequency shear wave impedance spectrometer for low viscosity liquids,” *Meas. Sci. Technol.* **12**(4), 519–524 (2001).
- ²⁵E. Benes, M. Gröschl, W. Burger, and M. Schmid, “Sensors based on piezoelectric resonators,” *Sens. Actuators, A* **48**, 1–21 (1995).
- ²⁶C. C. White and J. L. Schrag, “Theoretical predictions for the mechanical response of a model quartz crystal microbalance to two viscoelastic media: A thin sample layer and surrounding bath medium,” *J. Chem. Phys.* **111**(24), 11192–11206 (1999).
- ²⁷J. Munro and C. Frank, “Polyacrylamide adsorption from aqueous solutions on gold and silver surfaces monitored by the quartz crystal microbalance,” *Macromolecules* **37**(3), 925–938 (2004).
- ²⁸L. Qin, H. Cheng, J. M. Li, and Q.-M. Wang, “Characterization of polymer nanocomposite films using quartz thickness shear mode (TSM) acoustic wave sensor,” *Sens. Actuators, A* **136**(1), 111–117 (2007).
- ²⁹P. Resa, P. Castro, J. Rodríguez-López, and L. Elvira, “Broadband spike excitation method for in-liquid QCM sensors,” *Sens. Actuators, B* **166–167**, 275–280 (2012).
- ³⁰S. Rey-Mermet, R. Lanz, and P. Mural, “Bulk acoustic wave resonator operating at 8 GHz for gravimetric sensing of organic films,” *Sens. Actuators, B* **114**(2), 681–686 (2006).
- ³¹B. P. Sorokin, G. M. Kvashnin, A. V. Telichko, G. I. Gordeev, S. I. Burkov, and V. D. Blank, “Study of high overtone bulk acoustic resonators based on the Me1/AlN/Me2/(100) diamond piezoelectric layered structure,” *Acoust. Phys.* **61**(4), 422–433 (2015).
- ³²R. Thalhammer, S. Braun, B. Devcic-Kuhar, M. Gröschl, F. Trampler, E. Benes, H. Nowotny, and M. Kostal, “Viscosity sensor utilizing a piezoelectric thickness shear sandwich resonator,” *IEEE Trans. Ultrason., Ferroelect., Freq. Control* **45**(5), 1331–1340 (1998).
- ³³G. Wingqvist, H. Anderson, C. Lennartsson, T. Weissbach, V. Yantchev, and A. L. Spetz, “On the applicability of high frequency acoustic shear mode biosensing in view of thickness limitations set by the film resonance,” *Biosens. Bioelectron.* **24**(11), 3387–3390 (2009).
- ³⁴G. Wingqvist, J. Bjurström, L. Liljeholm, V. Yantchev, and I. Katardjiev, “Shear mode AlN thin film electro-acoustic resonant sensor operation in viscous media,” *Sens. Actuators, B* **123**(1), 466–473 (2007).
- ³⁵G. Wingqvist, “AlN-based sputter-deposited shear mode thin film bulk acoustic resonator (FBAR) for biosensor applications—A review,” *Surf. Coat. Technol.* **205**(5), 1279–1286 (2010).
- ³⁶G. Wingqvist, “Thin-film electro-acoustic sensors based on AlN and its alloys: Possibilities and limitations,” *Microsyst. Technol.* **18**(7–8), 1213–1223 (2012).
- ³⁷ANSI/IEEE 176-1987, *IEEE Standard on Piezoelectricity* (The Institute of Electrical and Electronics Engineers, Inc., New York, 1988).
- ³⁸C. Hauser, S. Radel, M. Gröschl, and E. Benes, “The influence of suspension and emulsion layers in ultrasonic BAW resonators,” in *Proceedings of Second Congress of Alps-Adria Acoustics Association and First Congress of Acoustical Society of Croatia* (2005), pp. 66–75.
- ³⁹V. Kurochkin and B. Sharfarets, “Resonances in the system ‘piezoelectric emitter-multilayer ultrasonic chamber with losses,’” *Acoust. Phys.* **55**(6), 918–924 (2009).
- ⁴⁰A. A. Kutsenko, A. L. Shuvalov, O. Poncelet, and A. N. Darinskii, “Tunable effective constants of the one-dimensional piezoelectric phononic crystal with internal connected electrodes,” *J. Acoust. Soc. Am.* **137**(2), 606–616 (2015).
- ⁴¹A. A. Kutsenko, A. L. Shuvalov, O. Poncelet, and A. N. Darinskii, “Quasistatic stopband and other unusual features of the spectrum of a one-dimensional piezoelectric phononic crystal controlled by negative capacitance,” *C. R. Mec.* **343**(12), 680–688 (2015).
- ⁴²H. F. Tiersten, *Linear Piezoelectric Plate Vibrations* (Plenum, New York, 1969).
- ⁴³R. Holland, “Representation of dielectric, elastic, and piezoelectric losses by complex coefficients,” *IEEE Trans. Sonics Ultrason.* **SU-14**(1), 18–20 (1967).
- ⁴⁴R. J. Williamson, “An improved method for measuring quartz crystal parameters,” *IEEE Trans. Ultrason., Ferroelect., Freq. Control* **34**(6), 681–689 (1987).
- ⁴⁵M. Schmid, E. Benes, W. Burger, and V. Kravchenko, “Motional capacitance of layered piezoelectric thickness-mode resonators,” *IEEE Trans. Ultrason., Ferroelect., Freq. Control* **38**(3), 199–206 (1991).
- ⁴⁶A. Amau, T. Sogorb, and Y. Jimenez, “A new method for continuous monitoring of series resonance frequency and simple determination of motional impedance parameters for loaded quartz-crystal resonators,” *IEEE Trans. Ultrason., Ferroelect., Freq. Control* **48**(2), 617–623 (2001).
- ⁴⁷R. W. Cemosek, S. J. Martin, H. L. Bandey, and A. R. Hillman, “Equivalent-circuit model for the TSM resonator with a viscoelastic layer,” in *Proceedings—Euroensors XIII, the 13th European Conference on Solid-State Transducers*, The Hague, The Netherlands (September 12–15, 1999).
- ⁴⁸S. J. Martin, H. L. Bandey, R. W. Cemosek, A. R. Hillman, and M. J. Brown, “Equivalent-circuit model for the thickness-shear mode resonator with a viscoelastic film near film resonance,” *Anal. Chem.* **72**(1), 141–149 (2000).
- ⁴⁹A. Menon, R. Zhou, and F. Josse, “Coated-quartz crystal resonator (QCR) sensors for on-line detection of organic contaminants in water,” *IEEE Trans. Ultrason., Ferroelect., Freq. Control* **45**(5), 1416–1426 (1998).
- ⁵⁰F. Coulouvrat, “On the equations of nonlinear acoustics,” *J. Acoust.* **5**, 321–359 (1992), available at <http://pascal-francis.inist.fr/vibad/index.php?action=getRecordDetail&idt=6126604>.
- ⁵¹P. A. Thompson, *Compressible-Fluid Dynamics* (McGraw-Hill, New York, 1972).
- ⁵²K. K. Kanazawa and J. G. Gordon, “The oscillation frequency of a quartz resonator in contact with a liquid,” *Anal. Chim. Acta* **175**(C), 99–105 (1985).
- ⁵³L. D. Landau and E. M. Lifshitz, *Fluid Mechanics, Vol. 6 of Course of Theoretical Physics*, 2nd ed. (Pergamon, Oxford, 1987).
- ⁵⁴B. Jakoby, “Estimation of vibration amplitudes for resonating sensors immersed in liquids,” *Meas. Sci. Technol.* **20**(12), 124003 (2009).
- ⁵⁵See www.piceramic.de (Last viewed March 10, 2023).
- ⁵⁶See www.krystaly.cz (Last viewed March 10, 2023).